International Journal of
Molecular Sciences

MDPI

Article

A Histopathological Scheme for the Quantitative Scoring of Intervertebral Disc Degeneration and the Therapeutic Utility of Adult Mesenchymal Stem Cells for Intervertebral Disc Regeneration

Cindy C. Shu [1], Margaret M. Smith [1], Susan M. Smith [1], Andrew J. Dart [2], Christopher B. Little [1,3] and James Melrose [1,3,4,*]

1 Raymond Purves Bone and Joint Research Laboratory, Kolling Institute, Northern Sydney Local Health District, St. Leonards, NSW 2065, Australia; Cindy.shu@sydney.edu.au (C.C.S.); mobsmith@sydney.edu.au (M.M.S.); Susan.smith@sydney.edu.au (S.M.S.); christopher.little@sydney.edu.au (C.B.L.)
2 Faculty of Veterinary Science, University Veterinary Teaching Hospital, University of Sydney, Camden, NSW 2050, Australia; andrew.dart@sydney.edu.au
3 Sydney Medical School, Northern, The University of Sydney, Royal North Shore Hospital, St. Leonards, NSW 2065, Australia
4 Graduate School of Biomedical Engineering, University of New South Wales, Kensington, NSW 2052, Australia
* Correspondence: james.melrose@sydney.edu.au; Tel.: +61-2-9926-4806; Fax: +61-2-9926-5266

Academic Editor: Cory J. Xian
Received: 8 March 2017; Accepted: 8 May 2017; Published: 12 May 2017

Abstract: The purpose of this study was to develop a quantitative histopathological scoring scheme to evaluate disc degeneration and regeneration using an ovine annular lesion model of experimental disc degeneration. Toluidine blue and Haematoxylin and Eosin (H&E) staining were used to evaluate cellular morphology: (i) disc structure/lesion morphology; (ii) proteoglycan depletion; (iii) cellular morphology; (iv) blood vessel in-growth; (v) cell influx into lesion; and (vi) cystic degeneration/chondroid metaplasia. Three study groups were examined: 5 × 5 mm lesion; 6 × 20 mm lesion; and 6 × 20 mm lesion plus mesenchymal stem cell (MSC) treatment. Lumbar intervertebral discs (IVDs) were scored under categories (i–vi) to provide a cumulative score, which underwent statistical analysis using STATA software. Focal proteoglycan depletion was associated with 5 × 5 mm annular rim lesions, bifurcations, annular delamellation, concentric and radial annular tears and an early influx of blood vessels and cells around remodeling lesions but the inner lesion did not heal. Similar features in 6 × 20 mm lesions occurred over a 3–6-month post operative period. MSCs induced a strong recovery in discal pathology with a reduction in cumulative histopathology degeneracy score from 15.2 to 2.7 (p = 0.001) over a three-month recovery period but no recovery in carrier injected discs.

Keywords: histopathology scoring; AF; disc degeneration; IVD; quantitative histology

1. Introduction

The intervertebral disc (IVD) is a tough but intricately organized connective tissue which resists tension and weight bearing during axial and torsional spinal loading but also provides spinal stability and flexibility [1]. The IVD achieves these remarkable properties through the interplay of a number of connective tissues of disparate structure and function that collectively endow the composite IVD with its unique mechanical properties [2,3]. The outer regions of the IVD, the annulus

fibrosus (AF), is composed of collagen rich annular lamellae, which are arranged around a central proteoglycan rich region called the nucleus pulposus (NP). Superior and inferior endplates of hyaline cartilage, the cartilaginous endplates (CEPs), enclose the NP where it borders the spinal vertebrae. Collectively, this arrangement of connective tissues equips the IVD with unique weight-bearing capability [4]. The hydration provided by the hydrophilic proteoglycans of the NP afford viscoelastic and hydrodynamic properties which equip the IVD with its ability to act as a weight bearing cushion [5]. The major proteoglycan of the NP is a large chondroitin sulphate (CS)and keratan sulphate (KS)rich proteoglycan of the Hyalectan family called aggrecan [5–8]. Hyaluronan forms massive link-protein stabilized aggregates with aggrecan which have impressive water regain properties; the high concentration of aggrecan in the NP generate an internal hydrostatic pressure in the IVD which counters axial spinal loading [9]. Furthermore, bulging of the NP upon axial spinal loading results in load transfer to the annular lamellae which bulge and generate radial hoop stresses which dissipate shear stresses generated during axial loading of the spine. Type I collagen is the major fibrillar collagen of the AF with its concentration maximal in the outer annular lamellae. Type II collagen is also present in the AF but to a far lesser extent, the NP however is rich in type II collagen where type II fibrillar networks entrap the hyaluronan (HA)-aggrecan-link ternary complexes which are so important for discal biomechanical function [8–11]. Other, more minor, proteoglycans with specific roles to play in the composite IVD include members of the small leucine repeat proteoglycan (SLRP) family, decorin, biglycan, fibromodulin, lumican, and keratocan [12,13], the CS-hyalectan member, versican, the lubricative proteoglycan, lubricin, and the large modular HS/CS proteoglycan perlecan [14] (reviewed in [15]). With ageing and degeneration, proteoglycans are lost from the NP through proteolytic cleavage [16–19] and the IVD becomes progressively more dehydrated and less biomechanically competent [3]. The matrix metalloproteinases (MMPs) produced by disc cells are regulated by the mechanical microenvironment of the cells [17,18,20] and can predispose the IVD to further mechanical damage and the generation of a number of characteristic lesions primarily in the AF [21]. The loss of aggrecan from the IVD lessens its ability to swell and act as a weight-bearing cushion and traumatic mechanical damage to the NP may be irreversible, distinguishing degenerative disc disease (DDD) from normal aging of the IVD [22]. Loss of discal aggrecan also promotes angiogenesis, and may lead to the ingrowth of blood vessels and nociceptive nerves and perception of discogenic low back pain (LBP) [23,24].

Degenerative disc disease (DDD) is now recognized as a major global disorder which along with associated low back pain (LBP) will be of sufficient severity to warrant consultation with a physician and will affect 80% of the general population some time in their lifetime [25]. Unfortunately, there are no effective treatments available to treat this condition other than surgical intervention. DDD results in the generation of LBP in the biomechanically incompetent IVD and has major socioeconomic consequences (reviewed in [26]). In the last two decades, a number of biological agents have been evaluated as prospective therapeutic interventions for DDD and this has led to the identification of several promising therapeutic targets [27–29]. These compounds have the ability to induce cellular proliferation, matrix deposition, regulate MMP production and activation, regulate inflammation and modify vascular in-growth and cell viability [30]. HA oligosaccharides of 10–12 saccharide units (HA oligos) have been shown to upregulate anabolic gene expression, MMP-2 and MMP-9 synthesis and activation in vitro. *MMP1* and *MMP13*, *ADAMTS1*, *ACAN*, *COL1A1* and *COL2A1* gene expression were all up-regulated in an annular lesion model of DDD and promoted annular repair processes [31]. A 16-amino acid fragment of link protein (LinkN, DHLSDNYTLDHDRAIH) has been shown to promote matrix synthesis by the resident disc cell population [32–35] and stimulated MSC proliferation and differentiation and promoted IVD repair [36,37]. Peniel 2000 is 2 kDa biglycan derived peptide with the ability to inhibit TGF-β1 activity and has provided beneficial effects in the treatment of disc degeneration [38]. Resveratrol (3,5,4′-trihydroxy-*trans*-stilbene), a plant phenolic compound found in the skins of grapes, blueberries, and raspberries, also has beneficial properties with regard to the treatment of DDD [29,39,40]. A number of commonly prescribed anti-cholesterol lipid

lowering medications have also produced beneficial effects on disc cell metabolism of application in the treatment of DDD. Simvastin [28,41,42], ortovastatin, and lovastatin [41–45] display protective effects on the IVD. A flavonoid isolated from grapefruit (naringin) and component of the traditional Chinese herb *Rhizoma drynariae* (Gusuibu) [46] has potent anti-inflammatory and anti-oxidant properties [47] which upregulates NP cell proliferation and down-regulates tumour necrosis factor (TNF)-α activity but elevates BMP-2, aggrecan and type II collagen protein production and also upregulates *ACAN* and *SOX6* and decreases *MMP3* gene expression [48]. This indicates that naringin may be a useful therapeutic agent in the treatment of DDD. A number of studies have evaluated the use of mesenchymal stromal stem cells (MSCs) for the treatment of DDD [26,49–54] and a number of reviews have covered this area of repair biology [55–60]. The mode of action of how MSCs illicit their therapeutic response in-situ remains an unanswered question and this needs to be addressed before MSCs can be morally advocated as a routine therapeutic intervention for DDD. A recent study using MSCs isolated from vertebrae demonstrated that they exhibited paracrine effects in co-cultures with AF and NP cells [61]. MSCs down-regulated pro-inflammatory cytokine gene production in degenerate NP (IL-1α, IL-1β, IL-6, and TNF-α) and AF cells (IL-1α and IL-6) and promoted extracellular matrix deposition. Growth factor mRNA was also elevated in MSC co-cultures, epidermal growth factor (EGF) insulin-like growth factor (IGF)-1, osteogenic protein (OP)-1, growth and differentiation factor (GDF)-7 and transforming growth factor (TGF)-β were all up-regulated by NP cells and IGF-1, OP-1 and GDF-7 by AF cells. These therapeutic effects are in keeping with the use of growth factor therapy to induce biological repair of degenerate IVDs [62,63] and establishes a paracrine mode of action for MSCs.

The EuroDISC clinical trial [64] utiliszd expanded autologous disc cells in single level discectomy patients, 28 patients reported greater pain reduction at 24 months than a control group and their IVDs had increased fluid contents evident by magnetic resonance imaging (MRI). Percutaneous injection of expanded autologous MSCs in two non-controlled clinical trials has also demonstrated improved MRI T2 signal and clinical improvement [65,66]. Use of autologous bone marrow derived MSCs in two small groups of DDD patients resulted in clinical improvement in 9/10 patients while conservative treatment failed [65,66]. A phase II clinical trial conducted with adult bone marrow MSCs for the treatment of back pain [67] resulted in the majority of the treated patients achieving a significant reduction in LBP. This has led to a multi center Phase III MSC clinical trial in DDD patients in 25 centers throughout the USA.

A major hindrance in the assessment of the efficacy of such biological interventions has been the inadequacy of many of the small animal models so far developed to examine DDD (reviewed in [68,69]). Large animal models of DDD have been developed in sheep [70–72], goats [73–75], dogs [76–78], and pigs [79–81] and, of these, the sheep represents the gold standard large animal model. In 1990, Osti and colleagues developed a model of DDD induced by controlled anterolateral (5 × 5 mm) surgical defects over a 24 months post operative (PO) period [71]. A number of studies have used this model and demonstrated spatiotemporal changes in discal and paradiscal components such as the NP [72], cartilaginous end plates (CEPs) [82], facet joints [83] and vertebral bone adjacent to and distant from the lesion site [84], ingrowth of blood vessels and nerves [85], focal expression of fibroblast growth factor (FGF)-2, TGF-β1 and α-smooth muscle cell actin [86] by cell populations associated with annular remodeling and repair of the lesion site. In an effort to develop a more aggressive model and to minimize maintenance costs, a modified ovine large lesion model was developed in 2012 using a 6 × 20 mm lesion [70]. The mechanical destabilization so induced led to more rapid lesion development in the AF and degeneration of the NP over a three to 6 month PO period rather than the 18–24 months required in the Osti model [72]. With a 6 × 20 mm lesion, qRT-PCR gene profiling demonstrated an elevation in catabolic matrix gene (*MMP2*, *MMP3*, and *MMP13*; and *ADAMTS4* and *ADAMTS5*) expression, these features have also been described in pathological human IVDs [87–90] and shown to severely impact on the biomechanical competence of the IVD. In the present study we compared the histopathological features of DDD and developed a quantitative scoring scheme. The efficacy of MSCs in the promotion of discal repair could also be evaluated using this scoring scheme.

2. Results

Figure 1 depicts proteoglycan staining with toluidine blue/fast green in a sham operated two-year-old ovine lumbar IVD, in 4 μm vertical sections demonstrating normal disc structure and proteoglycan levels. The specific areas of interest are represented by the boxed areas in the macro view of an entire IVD and adjacent vertebral body segments at the top of the figure composite are also shown at higher magnification in Figure 1a–c. Proteoglycan staining is typically faint in the outermost annular lamellae (Figure 1a) but the intensity of metachromatic proteoglycan staining (purple) increases in the mid (Figure 1b) and inner lamellae and is maximal in the NP (Figure 1c). Alternate annular layers in the mid and inner AF are discernable due to differences in staining intensity with toluidine blue and its merging with the NP (Figure 1d). Translamellar cross bridges also stain up with toluidine blue, indicating there is proteoglycan deposition in these structures (arrows) which provide interconnectivity between annular layers (Figure 1e,f). The cells are dispersed singly throughout the annular layers and are discernable as typical fibrochondrocytes, occasional doublet cells and small strings of cells arranged in arcade like arrangements along the lines of fibrillar lamellar collagens in the transitional zone where the inner AF lamellae merge with the NP (Figure 1c).

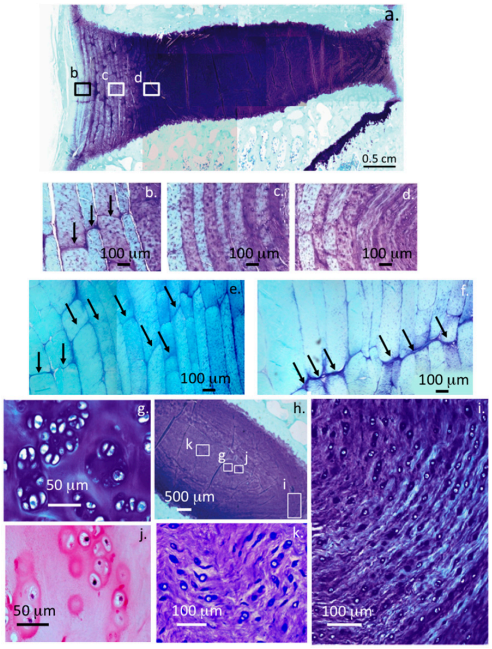

Figure 1. A Toluidine blue-fast green stained macroscopic view in vertical views of 4 μm sections of a two-year-ovine IVD (**a**); the boxed areas b, c, and d are also presented at higher magnification to provide detail of the tissue organization and cellular morphologies (**b**–**d**); translamellar cross-bridge formations (arrows) in the outer and inner AF of a three-year-old ovine IVD (**e**,**f**) stain positively with toluidine blue; isolated small clones of chondroid cells are also occasionally evident centrally in the NP (**g**,**h**,**j**); while normal NP cells are single (**k**); occasional cell doublets are evident in the inner AF (**i**).

Proteoglycan staining is maximal in the NP as evident in the low power view provided in Figure 1a. The morphology of the NP cells are typical of the small fibrochondrocytic observed elsewhere in the IVD however occasional small chondroid cell nests are discernable in some cases these differ from the typical resident NP cells (Figure 1k) since they are frequently seen to be dividing in these nests and are surrounded by a more extensive dense and non-fibrous basophilic matrix (Figure 1g,j). Furthermore, while very little fibrous material is in evidence in such chondroid cell nests, these are a prominent feature around the resident NP cells (Figure 1k). Detail of the cellular arrangements in the NP margins/transitional zone demonstrate the presence of some doublet cells and small strings

of interconnected fibrochondrocytes laid down in arcade type patterns following the distribution of fibrillar lamellar collagens (Figure 1i). Proteoglycans are also heavily stained with toluidine blue in the transitional zone (Figure 1i). The CEP contains cells of a rounded chondrocyte-like morphology in a proteoglycan rich matrix typical of a hyaline cartilage (Figure 2a,b) and can be differentiated from the adjacent IVD tissues where fibrous material is more prominent and the cells are smaller. H&E stained samples of CEP clearly depict the demarcation between CEP and adjacent vertebral bone, occasional blood vessels penetrating the CEP into the vertebral body are a normal feature and serve as a nutritional route for IVD cells (Figure 2a). The AF attaches to the CEP by a series of fibrillar attachments into the vertebral bone (Figure 2c,d). Cystic degeneration was also evident in a few IVDs at the margins of the NP/CEP where proteoglycans were depleted and cells were dead (Figure 2e).

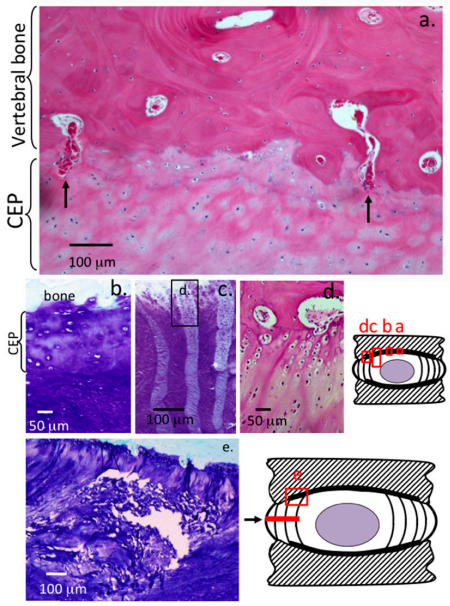

Figure 2. Histological detail of the cartilaginous endplate (CEP) and adjacent vertebral bone and annular attachment regions in a 4 µm thick vertical sections of normal lumbar three-year-old ovine IVD. H&E stained section with two blood vessels penetrating through the CEP arrowed (**a**); a similar region of the central NP CEP is depicted stained with toluidine blue (**b**); the CEP of the mid AF with annular attachments alternately stained (**c**); and a higher power view of a central region in (**c**) depicted as an H&E stained section in (**d**); an area of cystic degeneration adjacent to the central CEP (**e**) is also depicted and the area of the disc affected indicated in a disc schematic (**e**). The cartoons depict the areas of interest in the IVD shown elsewhere in this figure. Abbreviations: BV, blood vessel; CEP, cartilaginous endplate. Segments (**c**,**d**) modified from [91].

Schematic depictions of the 5 × 5 and 6 × 20 mm lesions in vertical and plan view (Figure 3a,i) and how the oblique sections of the lesion site perpendicular to the lesion zone were sampled. A 5 × 5 mm deep (Figure 3b) and 6 × 20 mm (Figure 3j) anterolateral transverse lesion cut in the outer AF of a cadaveric IVD followed by immediate histological processing including toluidine blue staining showed the appearance of these lesions without allowing any time for them to propagate further into the AF (Figure 3b,i). Longitudinal assessment of the 5 × 5 mm lesion discs over three to twenty-four months PO (Figure 3c–h) demonstrated a focal loss of proteoglycan in the outer AF lesion site at three months PO (Figure 3c,d); by six months PO (Figure 3e), the clearing of proteoglycans from the lesion site and inversion of the annular lamellae was more pronounced and small defects propagating from the original lesion were evident including delaminations and the start of circumferential tear development (Figure 3e). Lesion development was even more advanced at 12 and 18 months PO (Figure 3f,g), again focal loss of proteoglycan from the lesion site was a prominent feature and a

reduction in disc height and toluidine blue staining in the NP was also evident. By 24 month PO, the lesion had now developed through the NP to the contralateral AF, focal loss of proteoglycans in the outer AF of the original lesion site was still evident (Figure 3h). The relative size and location of the antero-posterolateral 6 × 20 mm IVD lesion is represented schematically in Figure 3i, and shown in a freshly cut and processed cadaveric disc (Figure 3j), compared to a non-operated control (NOC) disc (Figure 3k). There was no focal loss of toluidine staining in the lesion site since this is a time dependent process mediated by the cells in the lesion site, which are subject to alterations in the biomechanical micro-environment which modulates cell gene expression. Examination of the proteoglycan staining in the lesion affected IVDs three months PO revealed focal depletion of proteoglycans from the outer AF and propagation of the lesion into the NP (Figure 3l–n). A reduced disc height was also clearly evident and focal chondroid metaplasia of the outer AF (Figure 3l,m). Reduced proteoglycan staining was also evident in the NP of the 6 × 20 mm lesion affected IVDs three months PO (Figure 3l–n).

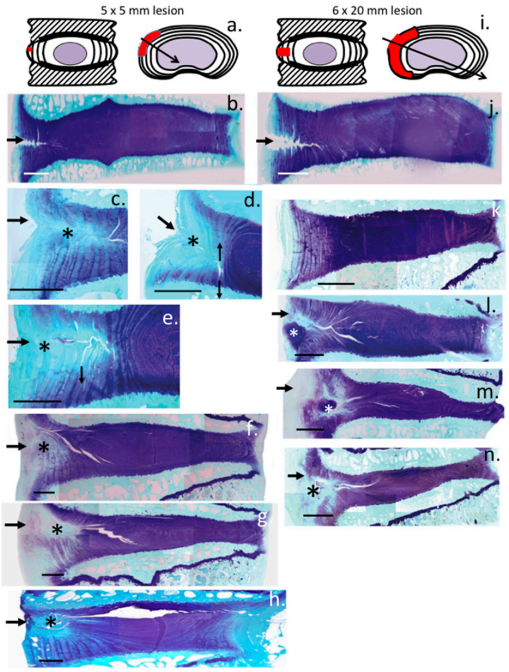

Figure 3. Histological appearance of IVDs affected by transverse outer annular lesions (arrows) in 4 µm vertical sections taken perpendicularly through the lesion zone. The sections taken are indicated in the schematics at the top of the figure with an arrow running through the lesion site depicting the oblique tissue sections sampled through the lesion site. Schematics depict IVDs and the 5 × 5 mm (**a**); and 6 × 20 mm lesion (**i**) used in this study, with the extent of the experimental defects indicated by colored red areas; Proteoglycan localization by toluidine blue-fast green staining are shown in vertical oblique sections of IVDs at various time-points post-lesion induction in the: 5 × 5 mm (**b**–**h**); and 6 × 20 mm lesion (**k**–**n**) DDD models; Toluidine blue/fast green stained vertical oblique sections of two-year-old (**b**–**h**) lumbar ovine IVDs. The arrows on the left hand side of each photosegment depict the original lesion site; Segment (**b**) is a non-operated control (NOC) disc in which a 5 × 5 mm lesion had been made just prior to histology; Segment (**j**) is a NOC disc in which a 6 × 20 mm lesion had been made; The 5 × 5 mm lesion IVD sections sampled: three months post-operation (PO) (**c**,**d**); six months PO (**e**); twelve months PO (**f**); eighteen months PO (**g**); and twenty-four months PO (**h**). Areas labeled with a black asterisk in (**c**–**h**) indicate focal areas of proteoglycan depletion. Notice the significant reduction in disc height twelve to eighteen months PO in lesion IVDs (**f**,**g**) and partial recovery and propagation of the defect over time into the contralateral AF (**h**). Three months post operative 6 × 20 mm lesion IVDs are also presented for comparison (**l**–**n**); and a NOC disc is presented in (**k**) for comparison. White asterisks in (**l**,**m**) represent areas of chondroid metaplasia, and the black asterisk in (**n**) represents focal proteoglycan depletion. Scale bars in the histology images are 500 µm.

A schematic diagram of the 5 × 5 mm (Figure 4a,b) and 6 × 20 mm lesion (Figure 4c,d) and how these propagate through the IVD over time was constructed to summarize these changes (Figure 4e-h).

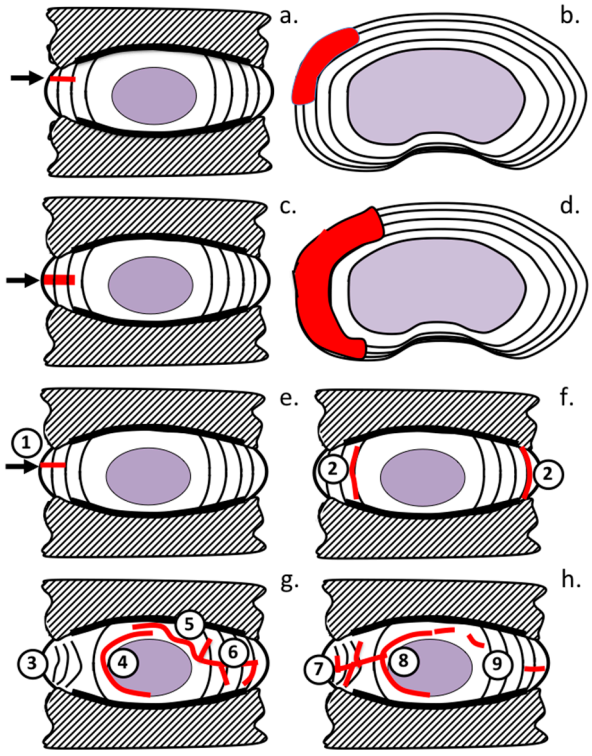

Figure 4. Schematic depiction of anterolateral lesion types used to initiate experimental IVDD: 5 × 5 mm lesion (**a**,**b**); and 6 × 20 mm lesion (**c**,**d**). A summary of the time dependent changes in lesion morphology in the: 5 × 5 mm lesion (**e**–**g**); and 6 × 20 mm lesion models (**h**) with lesions indicated in red. These include: rim lesions (1); radiating tears (2); annular inversion (3); propagation of radiating tears around NP (4); and into contralateral AF (5); development of delaminations (6); early development of delaminations in outer AF in 6 × 20 mm lesion (7); and propagation of radial tears around NP (8); and into contralateral AF (9).

A re-examination of the cellular morphologies at medium power magnification in the outer, mid and inner AF and NP of NOC IVDs stained with H&E showed a relatively disperse collection of single cells, doublet cells were also seen but only very occasionally in the inner AF (Figure 5a–d). Occasional chondroid cell nests were also observed in the NP however in the case shown in Figure 5 (insert) most of the cells were dead. These resembled the cell nests reported in Figure 1g,j. The antero-lateral annular lesions in the 5 × 5 mm lesion at 12 months PO (Figure 5e) and the 6 × 20 mm lesion at three months PO (Figure 5f) contained a large influx of cells and blood vessels. Small cell clusters were also observed near the 6 × 20 mm lesions (Figure 5g,h) similar to the chondroid cell nests previously described in the NP of NOC IVDs (Figure 1g,j).

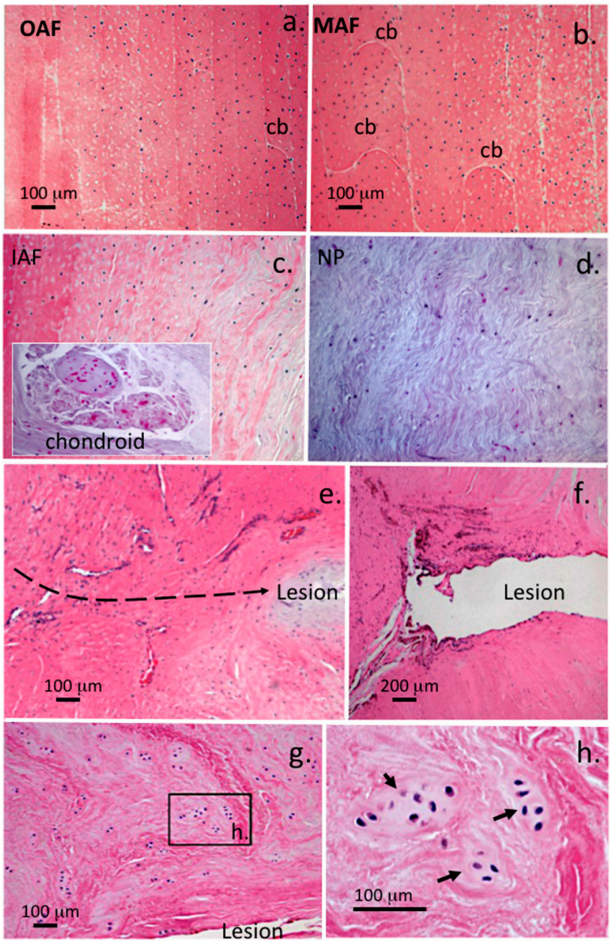

Figure 5. Comparison of the cellular distributions and morphologies in the: outer (OAF) (**a**); mid (MAF) (**b**); inner AF (IAF) (**c**); and NP (**d**) of a NOC ovine lumbar IVD compared to two examples of lesion affected IVD specimens stained with H&E (**e**,**f**); four micron thick vertical sections are depicted, with areas of the transverse lesion in (**e**–**g**); an influx of blood vessels and cells associated with the 5 × 5 mm lesion twelve month PO (**e**) and the unhealed inner AF in a 6 × 20 mm lesion three months PO (**f**); cell cloning adjacent to the lesion site was evident in the 6 × 20 mm lesion discs (**g**,**h**). The boxed area in (**g**) is presented in higher magnification in segment (**h**). Small chondroid cell nests were also occasionally observed in the NOC NP however in the example shown (panel **c** insert) these cells appeared to be dead. Abbreviations: cb, translamellar cross bridge. Scale bars shown are 100 μm, plates **c** and **d** are shown at the same magnification as plates **a** and **b**. The dotted line in e depicts the propagation plane of the lesion.

A closer inspection of the lesion associated cellular populations around the 6 × 20 mm lesions in higher power images (Figure 6a,d,e) confirmed that small groups of cell nests in discrete basophilic matrices were located in close proximity to the non-healed annular lesions that had propagated into the inner AF and NP margins (Figure 6a,d,e), similar less prominent chondroid cell nests had previously been observed in some of the NOC NP specimens (Figure 1g,j). The largest cell nests in the lesion affected AF tended to be in areas where maximal proteoglycan depletion was also evident (Figure 6d,e). These cellular morphologies were not a prominent feature of the Osti lesion affected IVDs but were evident in the 6 × 20 mm lesion IVDs in the vicinity of the annular lesions (Figure 6a). These IVDs are also depicted schematically (Figure 6b,c). The NOC ovine IVD also contained a relatively sparse distribution of singlet fibrochondrocytes throughout the outer AF (Figures 1b and 5a), mid AF (Figures 1c and 5b), inner AF (Figures 1d and 5c) and NP (Figures 1k and 5d).

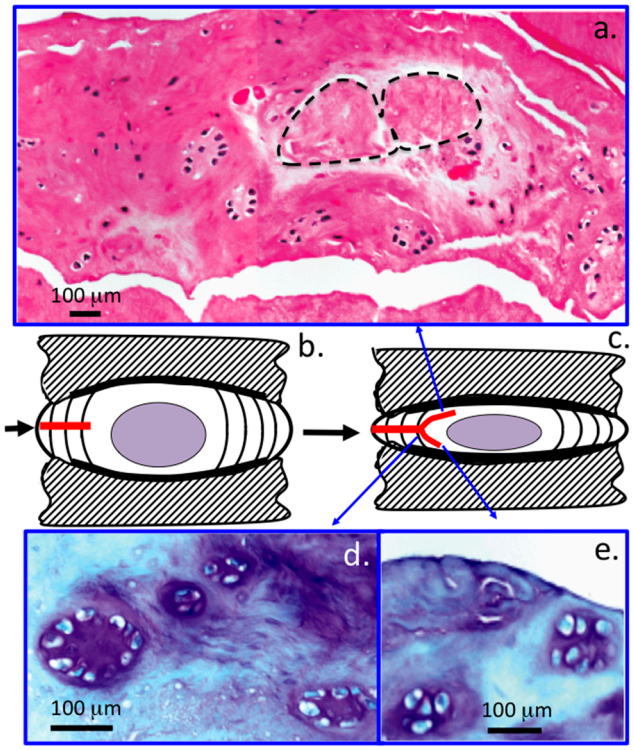

Figure 6. Histological assessment of cellular morphologies in ovine IVDs in: H&E (**a**); and toluidine blue-fast green stained tissue sections, 4 µm sections (**d**,**e**) in a 6 × 20 mm lesion at three months post lesion induction; schematic depictions of the lesion affected IVD are also shown in (**b**,**c**) showing the initial lesion site and its propagation by three month post surgery; small clones of cells are clearly evident in the vicinity of the annular lesion (**a**,**d**,**e**). Areas of tissue necrosis surrounded by dotted lines are also apparent in (**a**). Segment (**d**) is modified from [70].

An influx of blood vessels was also a prominent feature of the 5 × 5 mm (Figure 7a,b and Figure 8a,b) and 6 × 20 mm annular lesions (Figure 9a–c).

In the early stages of disc degeneration between 3–6 months PO in the 5 × 5 mm lesion discs blood vessels were prominent in the outer AF (Figure 7c,d) but were very rare in age matched normal IVDs, when rarely seen in NOC IVDs, the blood vessels rarely penetrated past the outermost collagenous lamellae. By 12 months post induction of the annular lesion, blood vessels had penetrated throughout the AF to the unhealed lesion site in the inner AF (Figure 8b). The 6 × 20 mm annular lesions had a similar ingrowth of blood vessels and associated cell populations to those seen in the 12 months 5 × 5 mm lesions; however, in the 6 × 20 mm lesion model, this occurred by three months PO (Figure 9a–c).

Many of these vessels contained entrapped red blood cells confirming their identity, fortuitously the red blood cells stained a prominent pink color with the H&E stain and could be easily identified. By 24 months in the 5 × 5 mm lesions, this cellular influx and blood vessels had regressed and the cell distribution in these tissues now resembled those of age matched IVDs.

The 6 × 20 mm lesion affected IVDs had a significant influx of cells and blood vessels into the AF (Figure 10a) and around the lesion site (Figure 10b,c) resembling that evident in the 5 × 5 mm lesion IVDs at 12 months PO (Figure 8b).

Focal loss of proteoglycan around the penetrating lesion was evident in the inner AF (Figure 11a) however occasional areas of intense toluidine blue staining due to chondroid metaplasia and focal proliferation of chondrocyte like cells (Figure 11b) was also evident in some cases. This contrasted with the small cell clusters in areas of the proteoglycan depleted lesion in the inner AF.

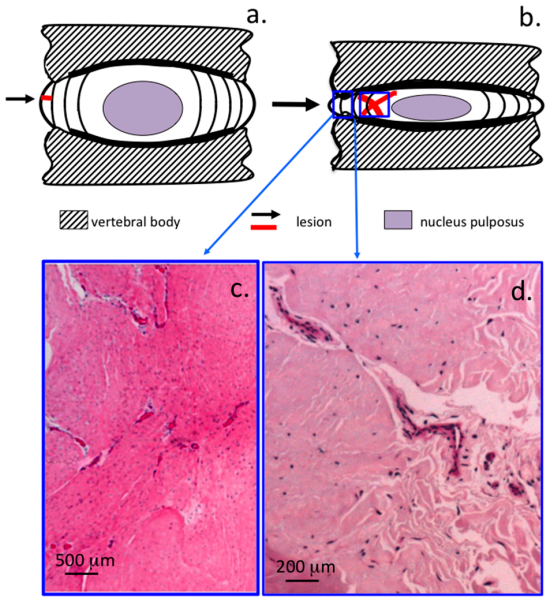

Figure 7. Diagrammatic representation of 5 × 5 mm anterolateral lesion affected IVD at: three (**a**); and six months (**b**) post lesion induction in 4 µm thick vertical IVD sections. Hematoxylin and eosin stained vertical sections of the AF are also shown of the blue colored boxed areas indicated in (**b**); in photosegments (**c**,**d**), an influx of blood vessels in the outer AF has undergone partial healing (**c**); however the lesion is still clearly evident in the inner AF (**d**).

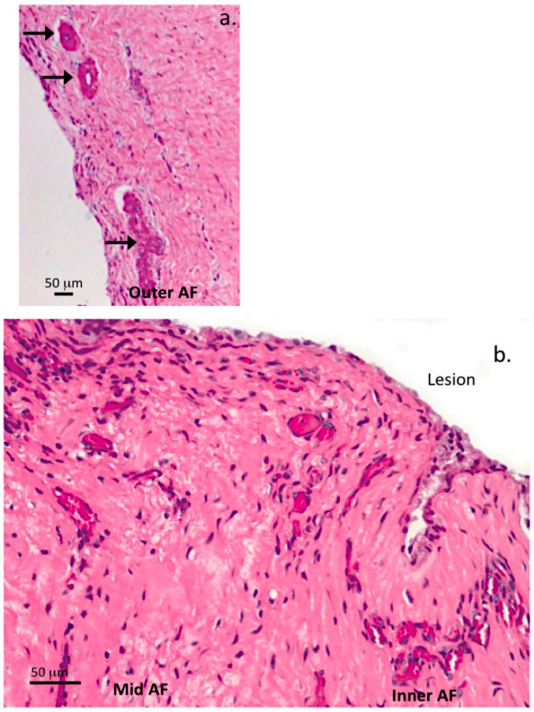

Figure 8. Visualization of blood vessels in transverse lesion affected IVDs, vertical 4 µm thick IVD sections. H&E stained vertical tissue sections through a lesion site outer AF, 5 × 5 mm lesion 6 months PO (**a**); and inner AF adjacent to a lesion site 5 × 5 mm lesion twelve month PO (**b**), demonstrating a few large prominent blood vessels (arrows) in the outer AF, a moderate influx of cells along the lesion track (**a**) and large influx of blood vessels with pink stained entrapped red blood cells and heavy infiltration of cells along the lesion site in the inner AF (**b**).

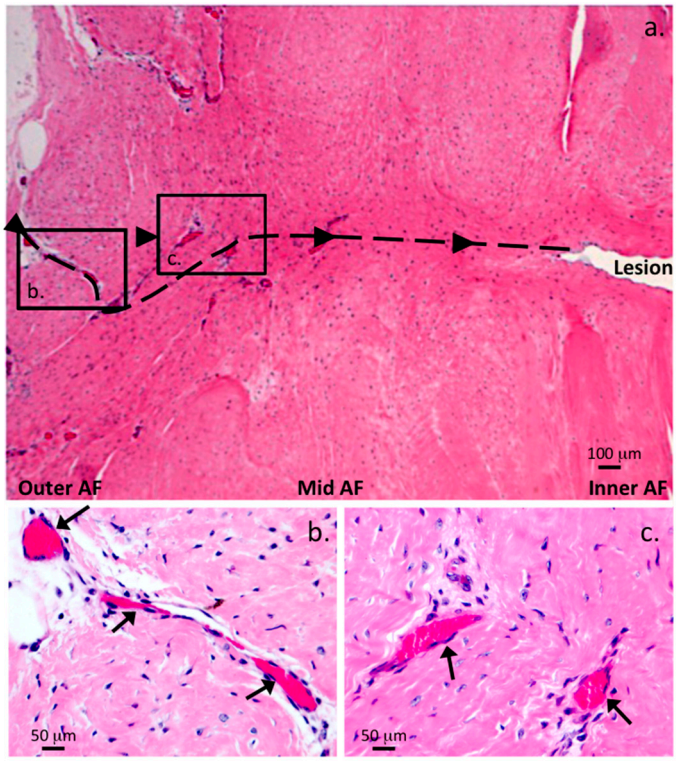

Figure 9. Immunohistochemical visualization of blood vessels and cellular influx into the 6 × 20 mm annular lesion site in 4 μm vertical IVD sections. Low power H&E stained vertical IVD section demonstrating the numerous blood vessels and cellular influx throughout the AF three months PO. Higher power views of two selected boxed areas in (**a**) are also presented showing the vessels (arrows) and entrapped red blood cells stained bright pink (**b**,**c**). A prominent influx of fibroblastic cells throughout the outer lesion site repair tissue is also a prominent feature in the AF but less so around the non-healed inner lesion site in this specimen. The propagation pathway of the lesion is depicted with a dotted line in (**a**), boxed areas are depicted at higher magnification below. The dense pink stained regions are entrapped red blood cells which intensely take up the H&E stain.

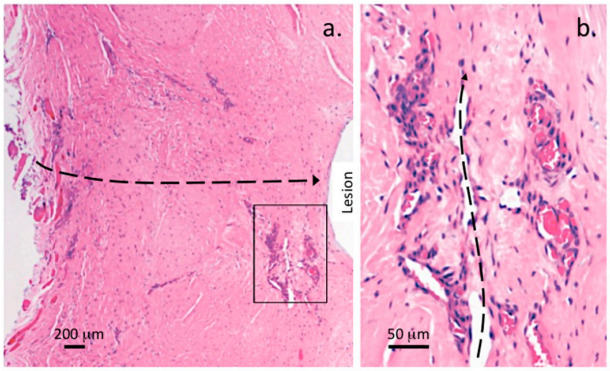

Figure 10. *Cont.*

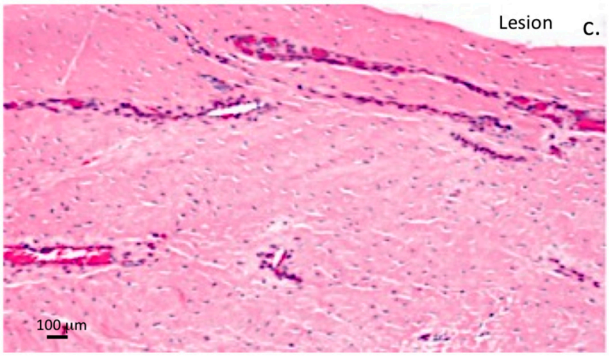

Figure 10. Low and medium power H&E stained 4 µm thick vertical disc sections through two lesion sites depicting prominent blood vessels in the outer AF with entrapped red blood cells stained prominently and the major influx of fibroblastic cells throughout the lesion site of a 6 × 20 mm lesion affected IVD (**a**) and prominently associated with vessels adjacent to the non-healed lesion in the inner AF, boxed area in (**a**); presented at higher magnification (**b**); A prominent longitudinally sectioned blood vessel (arrows) associated with a non-healed lesion in the mid AF is also evident with a moderate influx of cells around the lesion (**c**). The dotted lines in (**a**,**b**) depict the original pathway of the outer lesion (**a**) or vascularized unhealed inner lesion (**b**).

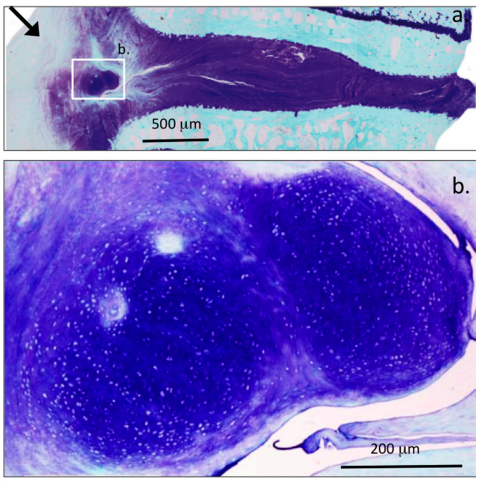

Figure 11. Toluidine blue histology of a 4 µm thick vertical disc section demonstrating proteoglycan localization (**a**); and a region of chondroid metaplasia (**b**) associated with the annular lesion site in a 6 × 20 mm lesion affected IVD at six months PO demonstrating high levels of proteoglycan production by cells of a rounded chondrocyte-like morphology. The arrow in (**a**) depicts the original site of the outer annular lesion.

The histopathology scoring scheme outlined in Table 1 was applied to disc sections from the 5 × 5 mm and 6 × 20 mm lesion models (Figure 12A–C). This showed differences between the two models in each of the discriminative parameters used in the histopathology scoring scheme and the more aggressive disc degeneration induced by the 6 × 20 mm lesion (Figure 12A). Administration of MSCs into lesion discs where DD had been induced three months earlier had followed by a three-month recuperative period resulted in a dramatic resolution of the degenerative features in these lesion discs. This was evident as a drop in the cumulative histopathology score from 15.7 to 2.0, close to the score for NOC IVDs and was statistically significant $p = 0.001$ (Figure 12C). Histology plates in Figure 12 clearly show that PBS carrier alone was an ineffective therapeutic agent with the annular lesion propagating through to and around the NP a very significant reduction in disc height was also evident (Figure 12D). The MSC injected IVDs, however, re-attained a near normal disc height and the annular lesion was

barely discernable, a significant therapeutic achievement reflected in a decrease of the histopathology degeneracy score from 15.7 to 2.0 (Figure 12E).

Table 1. Histopathological scoring of normal and pathological ovine IVDs. Abbreviations: IAF, inner AF; MAF, mid AF; OAF, outer AF; NP, nucleus pulposus; CEP, cartilaginous endplate.

Grade	Histopathological Features
	A. Toluidine Blue/Fast Green Proteoglycan Staining
0	Fast green staining only of OAF, metachromatic Toluidine blue staining of IAF, intense metachromatic staining in NP, well defined CEP staining. Alternate AF lamellae discernable due to differing metachromatic staining intensities of adjacent lamellae
1	Moderately reduced metachromatic staining of MAF/IAF in vicinity of lesion, fast green staining of OAF only, normal metachromatic staining of NP and CEP
2	Reduced patchy metachromatic staining around lesion, fast green staining in OAF (no metachromasia)
3	Reduced metachromatic staining in NP compared to sham or NOC IVD, very faint or no metachromatic staining in OAF/MAF, fast green staining only in OAF
	B. IVD Structure/Lesion Characteristics
0	Normal IVD structure with well defined annular lamellae, central NP and CEP
1	Lesion evident in MAF, normal NP morphology
2	Lesion evident in MAF/IAF, lesion but may not be apparent in OAF due to spontaneous repair, IAF lamellae may be inverted and have anomalous distortions in normal lamellar architecture
3	Bifurcation/propagation of lesion from MAF/IAF into NP margins, mild delamination, when more extensive may lead to concentric tears between lamellae in MAF/IAF
4	Propagation of lesion into NP, with disruption in normal NP structure, distortion of annular lamellae into atypical arrangements-severe delamination, separation of translamellar cross bridges
5	Lesion reaching through NP into contralateral posterior AF with disruption in normal NP structure
	C. Cellular morphology
0	Normal, sparse distribution of typical single AF and NP fibrochondrocytes
1	Small groups of rounded chondrocytic cells (two to four cells/group) in vicinity of annular lesion in IAF, occasional cell division in resident inner AF and NP cells
2	Moderate increase in well defined groups of rounded dividing cells (four to eight per group) in vicinity of lesion and with penetrating blood vessels associated with the lesion site, well defined chondroid cell colonies in NP contained within a dense basophilic matrix with little fibrillar material evident around the cells contrasting with NP cells
3	Numerous cell clones around IAF/MAF lesion, chondroid cell nests in NP containing >50 cells
	D. Blood Vessel Ingrowth
0	Very occasional vessels in outermost annular lamellae, occasional capillaries in CEP
1	Occasional blood vessels in OAF and MAF
2	Moderate number of blood vessels in IAF
3	Extensive ingrowth of vessels in IAF/MAF and along lesion margins
	E. Influx of cells into the lesion site
0	Normal cell distribution in OAF, MAF, IAF and NP
1	Slight influx of cells mainly in outer AF
2	Moderate influx of cells throughout AF
3	Large influx of cells throughout AF
4	Heavy influx of cells throughout AF particularly in inner AF and around lesion
	F. Histolopathological features not covered elsewhere
2	Chondroid metaplasia in AF
2	Cystic degeneration affecting ≥5% NP
3	Extensive cystic degeneration affecting ≥20% NP
4	"Bare" fibrillar elements in NP due to loss of ground substance, confirmed by a paucity of toluidine blue metachromasia affecting ≥20% of NP and also evident as a reduced disc height

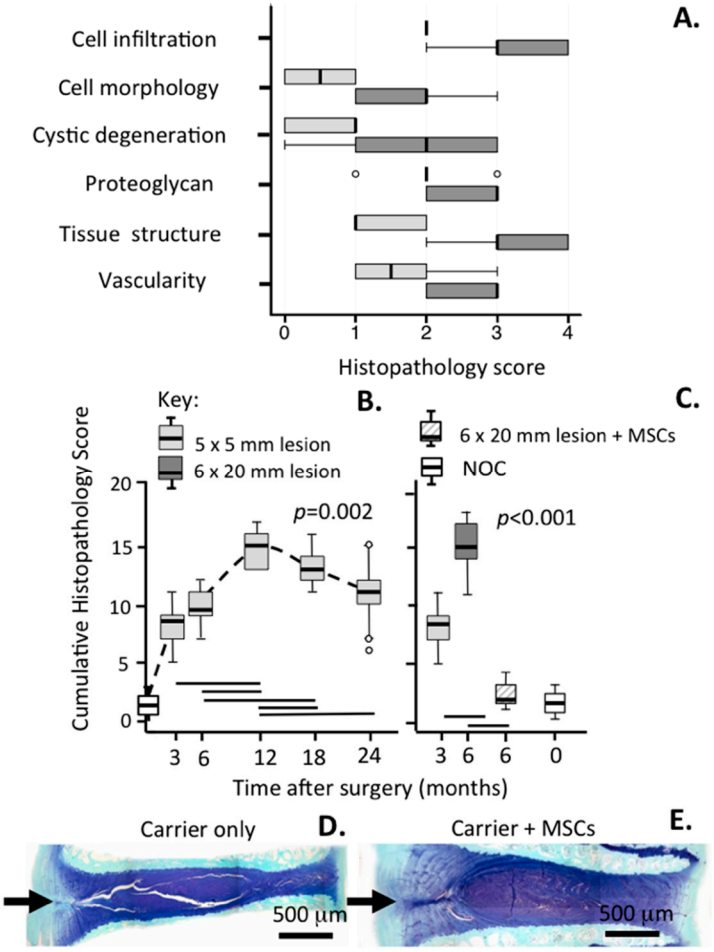

Figure 12. Histopathological scoring of IVDs from the 5 × 5 mm and 6 × 20 mm lesion models of experimental disc degeneration. The range of individual parameters which were scored for the cumulative histopathology score are indicated in (**A**); Longitudinal scores for the 5 × 5 mm lesion model up to 24 months post surgery are indicated in (**B**) and in the 6 × 20 mm lesion in (**C**). Overall, the time points for appearance of DDD are significantly different (Kruskal–Wallis rank test; $p = 0.002$ for **B** and $p < 0.001$ for **C**). A significant reduction in the cumulative histopathology score in the 6 × 20 mm lesion model from 15.7 to 2 was evident after administration of MSCs following a three-month period with an anterolateral lesion to induce degeneration and a three-month recovery period with MSCs (**C**). This was statistically significant ($p = 0.001$). NOC = non operated control. Histological sections of lesion affected discs stained with toluidine blue-fast green are depicted in (**D**,**E**). In (**D**), the lesion disc was injected with PBS carrier without stem cells; In (**E**), stem cells were injected; Notice the prominent lesion in (**D**) and significantly reduced disc height compared to (**E**) where a near normal disc height and almost complete disappearance of the lesion is evident, this disc however still had to attain the staining intensity of a NOC disc. The arrow in (**D**,**E**) depicts the original lesion site. For comparisons with a NOC disc see Figure 1a or Figure 2k. The bars above the *x* axes in (**B**,**C**) indicate significant differences between time points (Mann–Whitney *U* test; $p < 0.05$). In the box plots the centre line is median, box is 25%/75%; whiskers are 10%/90%; dots are outliers.

3. Discussion

Adams and Roughley proposed a useful definition of IVD degeneration as *an aberrant, cell-mediated response to progressive structural failure* [22]. Nociceptive nerve in-growth into degenerate human IVDs contribute to the perception of LBP [92] in ~40% of degenerate IVDs [25]. A recent ten-year global study, which surveyed 291 major human diseases, placed LBP as the number one musculoskeletal

disorder [93]. Approximately 80% of the general population in Western Societies is affected by LBP and its incidence increases with aging, peaking in the fifth and sixth decade [93]. In 1998, UK costings for the treatment of LBP were costed at £12.3 billion [94], in 2001 LBP cost $9.17 billion in Australia [95]. In 2006 the American Academy of Pain Medicine published costs for chronic pain in the USA at $560–635 billion/annually, 53% of all chronic pain patients had LBP and 31 million people were estimated to suffer from LBP at any one time [25,30,96]. In 1999, the World Health Organization (WHO) published the IRIS low back pain initiative [97] which highlighted LBP as a priority area and designated the development of biomaterials for disc replacement and stem cell methodology to restore functional IVDs as high priorites [26]. LBP was also made a National Research Priority Area by the National Health and Medical Research Council (NHMRC) and Australian Institute of Health and Welfare (AIHW) in 2009 [96] but to date have failed to fund any innovative projects designed to alleviate or better understand this condition. This is a major deficiency given the major and ever-increasing impact LBP makes on the Australian community [95,98]. Recent findings of the global burden of disease study 2010 [93] found that, of the 289 major human diseases examined, LBP ranked highest in terms of overall disability in terms of disability adjusted life years (DALYs) confirming the impact of LBP on the daily life of all individuals [99–101]. A number of animal models and preclinical studies have demonstrated the utility of MSCs for disc repair [37,61,69,102–105]. Phase I and II clinical trials with MSCs have already been completed and a phase III clinical trial is currently underway. In the USA.

Magnetic Resonance Imaging (MRI) shows ~40% of the general population display radiographic evidence of DD, a significant proportion of these patients suffer from LBP [106,107] suggesting that these conditions are causally linked [108–110]. LBP arising from DDD may be caused by inflammatory responses triggered by degenerate IVD tissue herniating into the spinal canal [111], nerve ingrowth into the IVD [110,112] or due to altered spinal biomechanics [113]. In terms of pain relief and recovery of spinal function, surgery (spinal fusion) remains the most effective treatment currently available but is associated with degenerative IVD changes adjacent to the fusion mass. Biological methods are also of interest as a treatment option [27,58,114–118]. A major hindrance to the assessment of the efficacy of such therapeutic strategies has been the inadequacy of the animal models available to examine DDD (reviewed in [68]). Large animal models of DDD have been developed in dogs [76,77,119], sheep [70–72], goats [73–75] and pigs [79–81]. The latter two species suffer from anomalously high spontaneous healing responses and persistence of notochordal cells in the IVD with ageing, compounding unequivocal interpretation of the efficacy of therapeutic repair strategies. Sheep and canine represent appropriate animal models for such evaluations relevant to the human condition. Spinal manipulation studies demonstrate annular lesions influence IVD biomechanics, neurophysiological responses, vertebral lumbar motion segment responses, muscular contributions to dynamic dorsoventral lumbar spinal stiffness and three-dimensional vertebral motion in lumbar spinal motion segments. Multifidus muscle remodeling [33,120–128] in response to DDD may also be a source of LBP. Changes in multifidis pro-inflammatory cytokine gene expression [127] occur in response to experimental DDD [70]. Similar changes in human spinal tissues and LBP have been reported with DDD [129] reinforcing the appropriateness of the ovine model for valid comparisons with the human spine.

Disc cells obtain their energy primarily by anaerobic glycolysis to generate adenosine triphosphate and lactic acid from glucose [130]. An adequate supply of glucose is an absolute requirement for disc cell nutrition. Disc cells die within 2–3 days under low glucose conditions [131]. Diffusive processes from peripheral blood vessels are a major nutritional pathway for disc cells and for the removal of metabolic waste products (lactate). Oxygen tensions of 5.8 KPa in the CEPs and outer AF and 2 KPa in the central NP in human IVDs have been measured. Lactate concentration gradients inversely mirror IVD O_2 tension profiles ranging from 2 mmol/L in the outer AF to 6 mmol/L in the center of the NP [132–134]. Lactic acid concentrations in the disc can reach 6–8 mM compared to 1 mM in plasma, leading to an acidic pH of 6.9–7.1 in IVDs. With DD, lactic acid concentrations can reach 20 mM and intradiscal pH values ~6.0 [135,136]. Matrix synthesis in the IVD ceases if the pH falls below 6.8 [136]

compromising disc cell viability and an impairment in disc tissue homeostasis [137–144]. This effect is more pronounced under conditions of low glucose concentrations (<0.5 mM). Degenerate IVDs with a pH < 6.5 are unsuitable candidates for repair using MSCs since at these pH values reduced cell proliferation, viability, an absence of matrix synthesis and lowered anabolic gene expression is evident. The pH in a healthy IVD varies between 7.0–7.2, but falls to 6.7–6.9 in a mildly degenerate IVD. Severely degenerate IVDs have a pH of 6.0–6.5. A pH below 6.8 in the IVD shuts down MSC cell proliferation and matrix production, thus it is important to determine the degenerative status of candidate IVDs to determine their suitability for MSC treatment. Improvements in IVD imaging facilitate the non-invasive determination of the degenerative status of an IVD based on its internal pH and glycosaminoglycan (GAG) profile and aids in patient selection [145,146].

In 1990, Osti and colleagues were awarded the Volvo Prize for the development of a model of DDD using controlled anterolateral (5 × 5 mm) surgical defects which induced DDD over a 12–18 month post operative (PO) period [71]. A number of studies using the Osti model have demonstrated that annular defects also impact on other discal and paradiscal components such as the NP [72], CEPs [82], facet joints [83] and vertebral bone adjacent to and distant from the lesion site [84]. The ingrowth of blood vessels and nerves [85] into experimentally injured IVDs and focal expression of FGF-2, TGF-β1 and α-smooth muscle cell actin [86] by cell populations associated with the lesion sites have also been demonstrated. The impact of lesion progression on disc proteoglycans has demonstrated degradation of aggrecan [147], upregulation of decorin and biglycan [148] and fragmentation of biglycan and fibromodulin [149]. In an effort to develop a more aggressive model of DDD in sheep a 6 × 20 mm annular lesion was used to induce DDD by three months post surgery rather than the 12–18 months PO in the Osti model [70]. The resultant mechanical destabilization induced de-lamellation, radial lesions, and bifurcation of the outer annular lesion, and anomalous modification of annular attachments to the CEP [150] similar to those identified in the Osti model [71] and in human DDD [87,90]. Altered discal biomechanics (Neutral zone, forward and lateral bending, torsion, range of motion) and qRT-PCR gene profiling of selected representative anabolic and catabolic matrix genes further demonstrated the utility of this model which closely reproduced defects described in pathological human IVDs [87–90]. These background studies were the impetus for the development of the histopathological scoring scheme described in the present study. This six-category scheme examined PG depletion, changes in annular structure and cellular morphology associated with experimental DD. The ingrowth of blood vessels and cellular influx into annular defect sites, chondroid metaplasia and cystic degeneration provided additional quantitative information on DD. This scheme was also useful for assessing changes in degenerate IVDs induced by administration of MSCs into a degenerate IVD resulting in a reduction in total histopathology score from 17.5 to 2.2 over a three-month recuperative period. This was a significant finding considering the large size of the degenerative lesion in this model and clearly demonstrated the regenerative power of MSCs.

A review of existing classification schemes for human DD published in PubMed from 1957–2016 uncovered 42 schemes, 30 of these dealt with the lumbar spine. Progressive stages of spinal degeneration affecting the IVDs, facet joints, vertebral bodies and spinal canal were described in these studies (reviewed in [151]). Five of these grading schemes used microscopic anatomy, four used histology, six used plain radiography and five MRI while three utilized discography to describe degenerative changes in spinal components. Other classification schemes have used combinations of these techniques plus biomechanics [152], MRI, biochemical composition, histology, radiography [153], or MRI and discography to score DDD [154,155]. Existing imaging methods such as X-ray, CT and MRI can reliably detect changes in the IVD with degeneration however they lack enough sensitivity to reliably detect the earliest stages of DDD. Novel MRI techniques such as magnetization transfer spinal imaging [156–159], chemical exchange saturation [145,146], ultrashort echo time MRI, and sodium MRI [160–165] are sensitive to ECM molecules such as proteoglycans and collagens and these newer imaging modalities hold promise in the detection of quantitative alterations in functional discal ECM components in the early stages of DDD [166,167]. Patients with identifiable early stages of DDD likely

to progress to a chronic stage are expected to be the most suitable candidates for biological therapeutic interventions to improve discal structure and function.

Kellgren and Lawrence (1957) [168] were the first to use radiography to classify degenerative changes in the osteoarthritic spine with grade 1 representing minimal anterior osteophytosis, grade 2 definite anterior osteophytosis and possible disc space narrowing and sclerosis of the vertebral plates. Grade 3 was characterised by moderate narrowing of the disc space, vertebral plate sclerosis and osteophytosis. Grade 4 described severe disc space narrowing, sclerosis of vertebral plates and multiple large osteophytes. The Kirkaldy-Willis classification scheme of 1978 [169] considered degenerative changes including spinal dysfunction, herniation, instability, lateral nerve entrapment, single and multiple level central spinal stenosis. Adams et al. (1986) [170] classified, stages of DD using discography and described, "cottonball" IVDs as those with no signs of AF degeneration but a soft white amorphous NP; "lobular" discs were a mature disc with the NP starting to coalesce into fibrous lumps; "Irregular", a degenerative disc with fissures and clefts in the NP and inner AF; "fissured" IVDs were degenerative discs with radial fissures stretching from the inner AF to the outer edge of the AF and "ruptured" IVDs contained a complete radial fissure allowing fluid to escape the IVD. Pathria et al. (1987) [171] developed a radiographic scheme to grade facet joint disease into 4 degenerative stages. Grade 0, normal; grade 1, facet joint space narrowing; grade 2, facet joint narrowing plus sclerosis or hypertrophy; grade 3, severe OA of the facet joint with narrowing, sclerosis and osteophytes. In 1988, Modic et al. [172,173] used T1 and T2 MRI to describe marrow changes in the vertebral bodies associated with DDD and categorized these into three stages (Modic type I–III). Type I, decreased T1 signal but increased T2 signal representing marrow edema associated with disruption and fissuring of the endplate and vascularized fibrous tissue within the adjacent marrow. Modic Type II, increased T1 signal and iso-intense or hypo-intense T2 signal due to fatty degeneration of subchondral marrow, endplate disruption with yellow marrow replacement in adjacent vertebral body. Modic Type III, decreased T1 and T2 signal correlated with extensive bony sclerosis on plain X-rays, dense woven bone with no marrow to produce MRI signal. MRI assessment of Modic changes due to vertebral bone lesions, indicated fatty marrow infiltration and inflammatory edematous changes in vertebral bone [174]. Thompson et al. (1990) [175] evaluated radiographic, morphologic and anatomical assessments of DDD and went on to correlate these with MRI and zonal IVD compositional changes. Weiner et al. (1994) developed a four-point classification scheme correlating radiographic spinal changes with alterations in spinal flexibility, progressive degenerative changes in facet joints and IVDs based on the extent of disc space narrowing, osteophyte formation and bone eburnation. Weishupt et al. (1999) [176] used MRI and CT to assess facet joint changes associated with DDD and developed a 4 point grading scheme based on facet joint narrowing, osteophyte development, hypertrophic changes in the articular processes, subarticular bony erosions and subchondral cysts. Pfirrmann et al. (2001) [177] used MRI to assess spinal degeneration concentrating on changes in the IVDs. The Pfirrmann scheme consists of 5 grades. Grade I, IVD homogeneous with a bright hyper-intense white signal intensity and a normal disc height. Grade II, IVD structure inhomogeneous with a hyper-intense white signal but clear distinction between NP and AF and normal disc height with or without horizontal grey bands. Grade III, IVD structure inhomogeneous with an intermediate grey signal intensity, unclear distinction between NP and AF, disc height normal or slightly decreased. Grade IV, IVD structure inhomogeneous, hypo-intense dark grey signal intensity, no distinction between NP and AF, disc height normal or moderately decreased. Grade V, IVD structure inhomogeneous, hypo-intense black signal intensity, no distinction between NP and AF, disc space collapsed. Carragee et al. (2003) [178] classified disc degeneration in terms of lumbar disc herniation classified into: (i) "fissure type", a herniation with minimal annular defect and extruded or sequestrated fragment; (ii) "defect type" herniation with a large or massive annular defect and an extruded or sequestrated fragment; (iii) "contained type", herniation with an intact AF and one or more sub-annular detached fragment; and (iv) "no-fragment, contained type" herniation with an intact AF and no sub-annular detached fragment. Thalgott et al. (2004) [179] developed a six-point classification system for DDD based on a combination of MRI,

provocative discography, plain X-rays and specific anatomic features which assessed spinal curvature and a 4 point assessment of facet joint degeneration. Most recently, Wang and colleagues (2012) [180] categorized changes in vertebral endplates and correlated these with age and the onset of DDD. In 2013 Rutges and colleagues (2013) [181] published a validated histological classification scheme to describe the various stages of human DDD. This is similar to a classification scheme for canine disc degeneration [76] and to the scheme we have developed in the present study but is less discriminative.

A number of studies have documented positive results with MSCs in disc repair [37,49,65,182–187] and this has also been the subject of a number of definitive reviews [26,58,188–191]. The results we obtained with MSCs in the ovine annular lesion model of experimental DD are therefore consistent with these earlier findings. Furthermore, the histopathological scoring we undertook of control and MSC treated tissues in the present study further reinforced the efficacy of MSCs as a therapeutic agent and the validity of the scoring system.

Intervertebral disc degeneration involves changes in many of its constituent tissues [22] and any prospective scheme aimed at scoring histopathological changes in this composite connective tissue must address each of these components and herein lies a major strength of the proposed new scoring scheme. While useful, most of the previously developed classifications of DDD are incapable of precisely identifying details of all of these aspects of DDD although recent improvements in X-ray, MRI and d-GEMRIC technology is correlating imaging modalities with supportive biochemical data [192]. Annular rim-lesions due to fatigue failure of the Sharpey fiber attachments of the annulus into the vertebral body rim are a common feature in DDD and these lesions may propagate into the inner AF and even through to the contralateral AF in extreme cases [21]. Bifurcation of the rim lesion due to separation of adjacent annular lamellae in the mid and inner AF are also evident in DD and may lead to development of radial fissures. These would be expected to severely impact on the ability of the AF to withstand the hoop stresses which it normally resists during axial spinal loading, and may actually be the driving forces which propagate annular lesions [193]. Focal loss of proteoglycan around annular lesions is also found in DDD and demonstrate changes in local catabolic processes by the resident disc cell populations presumably in response to changes in their biomechanical microenvironment produced by annular lesions [70]. An influx of cells to the annular lesion site occurs in IDD, some of these express TGF-β and FGF-2 [86] and these growth factors have roles in promoting the laying down of ECM components by the resident disc cells. FGF-2 is also an angiogenic growth factor and promotes the ingrowth of blood vessels into lesion affected degenerate IVDs [85]. Cell clustering also occurs in such regions of the IVD affected by annular lesions and may be a response by the resident stem cell populations [70]. Changes in the CEP (including cyst formation) can also contribute to DD through disruption in normal nutrient pathways to the disc cells [26]. Loss of proteoglycan from the NP in DD leads to a reduction in the ability of this tissue to resist compression and a reduction in disc height [194,195]. Taken together, it is clear that DDD is a multifactorial disorder and a histopathological scoring scheme must reflect this. The proposed scheme should be suitable for the description of DDD in any large animal and human IVD. Use of this scheme may further identify that like degenerative arthritic changes in OA and RA [196–203], DDD displays a spectrum of degenerative features and several sub-types of DDD are likely to be identified in the future when sufficient data is collected for critical evaluation. However for such a development to occur one must have a reliable, discriminative scoring scheme capable of evaluating the relative importance of each of the listed degenerative features of DDD. It is our contention that the proposed new classification scheme we have developed and described herein provides such a scheme.

4. Materials and Methods

The data reported in this study is based on studies conducted in 1992 [72] and 2012 [70] where 5 × 5 and 6 × 20 mm annular lesions were used to induce DDD in merino wethers, all methodology is provided in detail in these earlier publications. Ethical approval for conducting all animal

procedures was obtained from the Royal North Shore Hospital Animal Care and Ethics Committee of The University of Sydney in 1992 and in 2011 as outlined in earlier studies [70,72].

4.1. Ovine Models of DDD

Briefly, merino wethers aged 3–4 years of age were purchased at local sale yards. Sixty-four animals were used in the 5 × 5 mm lesion study, animals were randomly separated into 4 groups of 16 animals, 8 of the animals in each group received controlled anterolateral lesions in the L1L2, L3L4 and L5L6 IVDs, the remaining animals did not receive a lesion and served as sham operated controls (surgical approach only). All animals were maintained in open pasture and allowed to roam freely post surgery. The animals were subsequently sacrificed at 6, 12, 18 and 24 months post operatively (PO) and the spines removed (two additional sheep were also sacrificed 3 month PO). The IVDs of interest and adjacent vertebral body segments were isolated using a bone saw and fixed in 10% neutral buffered formalin. In the 6 × 20 mm lesion study group thirty-two merinos were separated into a lesion group and sham operated group. The Lesion group received 6 × 20 mm anterolateral lesions in the L1L2, L3L4 and L5L6 IVDs. Animals were sacrificed 3 month PO and the spines were excised and IVDs of interest isolated for histology.

4.2. Induction of Disc Degeneration and Administration of Mesenchymal Stem Cells

A total of 18 three-year-old merino wether sheep were divided into 3 groups (lesion plus two non-operated control (NOC) sheep groups). All of the animals (except NOC sheep) received 6 × 20 mm annular lesions at the L1L2, L3L4 and L5L6 spinal levels by our established model [70]. After 12 weeks to establish disc degeneration, a second surgery was performed to expose the contralateral AF away from the lesion site and 10 million MSCs in 0.2 mL PBS or PBS carrier were injected into the NP through the undamaged AF of the L1L2, L3L4 and L5L6 lesion IVDs. After a further 14 weeks recovery from surgery the sheep were sacrificed and the lumbar IVDs collected for histological examination.

4.3. Isolation and Characterization of Mesenchymal Stem Cells

Details of the isolation and demonstration of pluripotency of ovine mesenchymal stem cells from pooled iliac crest bone marrow are as noted earlier [204]. Frozen cell stocks were thawed from nitrogen storage and grown in monolayer culture for several passages to expand cell numbers, passage 8 cells were used in this study. The chondrogenic, adipogenic and osteogenic pluripotency of these MSCs was confirmed as indicated earlier prior to their use in the annular lesion model [204].

4.4. Histological Processing of IVDs

Prior to fixing the IVDs, all soft tissue surrounding the IVDs was trimmed off, the posterior elements were removed with bone cutters and most of the superior and inferior vertebral bodies adjacent to each IVD were trimmed off with bone saws. The remaining bone was trimmed down to ~1 mm from the margins of the IVD using a Dremel burring tool. En-bloc fixation of the IVDs was undertaken for 48 h in 10% neutral buffered formalin. The vertebral body margins attached to the IVD are essential for the preservation of native tissue architecture and prevention of artifactual swelling of IVD specimens during fixation [205]. However, it is also critical to minimize the amount of bone attached to the IVD specimens to cut down on the decalcification time for each specimen to ensure the preservation of cellular detail and antibody epitope reactivity for later immunolocalization studies. Decalcification was undertaken with 10% formic acid 5% neutral buffered formalin with constant agitation Vertical tissue blocks (~5 mm thick) were taken of the IVD-vertebral bodies perpendicular to the lesion sites. These tissue blocks were dehydrated in graded ethanols and xylene and embedded in paraffin wax. Due to the large size of the 6 × 20 mm lesion this was sampled at three sites across the lesion site to obtain representative samples and these were separately evaluated. Four-micron vertical tissue sections were cut and adhered to SuperFrost Plus microscope slides for histological

examination. Tissue sections were de-paraffinized in two changes of xylene prior to rehydration of the slides through graded ethanol washes (100–70%) to water.

4.5. Histochemistry

4.5.1. Toluidine Blue Staining

Vertical sections (4 μm) of IVD and superior and inferior vertebral bodies were stained for ten minutes with 0.04% w/v toluidine blue in 0.1 M sodium acetate buffer, pH 4.0, to visualize the glycosaminoglycans followed by a two minute counterstain in 0.1% w/v fast green FCF.

4.5.2. Hematoxylin and Eosin Staining

Tissue sections were stained in Mayers Hematoxylin (five minutes), rinsed in tap water blued in Scotts Blueing solution (one minute) and counterstained in 0.0001% eosin (5 min), dehydrated in 95% ethanol then absolute ethanol, cleared in xylene and mounted.

4.6. Development of a Histopathological Scoring System for IVD Specimens

An extensive 27 point six category histopathological scoring scheme (See Table 1) was developed based on: (i) toluidine blue proteoglycan localization; (ii) lesion structural characteristics; (iii) cellular morphology; (iv) extent of blood vessel ingrowth; (v) cell infiltration; and (vi) presence or absence of specific degenerative features such as cystic degeneration or chondroid metaplasia. These parameters were assessed in the outer, mid and inner AF, NP and contralateral AF of the lesion affected and sham operated IVDs.

4.7. Statistics

Power calculations from previous studies suggested there was a 90% power of detecting a four unit difference in histology score using six sheep per group. Histology scores were tested for significance using the Kruskal–Wallis (KW) equality-of-populations rank test in the first instance. If significance was found ($p < 0.05$), individual groups were compared using the Wilcoxon rank-sum test. Within each parameter, the Benjamini–Hochberg post hoc test was used to correct for false positives. All statistical analyses were performed using STATA 13 statistical software (Survey Designs, StataCorp LP, College Station, TX, USA). Data are presented as box plots with median values indicated with a solid horizontal bar

5. Conclusions

The histopathological scoring scheme described in the present study can be employed to quantitatively score IVD degeneration and regeneration following administration of adult MSCs and should also be applicable to the assessment of the efficacy of other biological interventions. Furthermore, this scheme can be used in conjunction with imaging (X-ray and MRI) and functional methods such as biomechanics and with biochemical compositional and gene expression techniques to examine these processes using a highly informative multidisciplinary approach.

Author Contributions: Cindy C. Shu assisted in the day to day running of the study, undertook MSC isolation and demonstration of pluripotency, maintained MSC cultures, undertook data collection and record keeping during sheep surgeries, histology scoring, reviewed versions of the manuscript, and approved the final version. Margaret M. Smith undertook statistical analyses, reviewed data interpretation, assisted in manuscript writing and review, histology scoring. Susan M. Smith undertook all histology work, assisted in interpretation of histology data, manuscript review. Andrew J. Dart undertook the sheep surgeries, supervised post operative care and maintenance of the sheep, contributed to manuscript writing, interpretation of data, manuscript review and input on all veterinary and animal welfare aspects of the study. Christopher B. Little assisted in the sheep surgeries and post operative care, had intellectual input into experimental design and interpretation of data, assisted in manuscript writing and review, contributed to a clinical overview of the significance of the findings. James Melrose was responsible for fund raising, writing of ethics applications and other reports on the study, co-ordination of research input from other candidates, liased with Andrew J. Dart to ensure animal welfare,

undertook manuscript writing and review, conceptualization of the study, had intellectual input on experimental design and interpretation of data, assisted in data recording, interpretation of histology and construction of figures, histopathology scoring. All participants reviewed and approved the final version of the manuscript.

Conflicts of Interest: The authors declare no conflict of interest or financial disclosures.

References

1. Humzah, M.D.; Soames, R.W. Human intervertebral disc: Structure and function. *Anat. Rec.* **1988**, *220*, 337–356. [CrossRef] [PubMed]
2. Iatridis, J.C.; MacLean, J.J.; Roughley, P.J.; Alini, M. Effects of mechanical loading on intervertebral disc metabolism in vivo. *J. Bone Jt. Surg. Am.* **2006**, *88* (Suppl. S2), 41–46. [CrossRef]
3. Roughley, P.J. Biology of intervertebral disc aging and degeneration: Involvement of the extracellular matrix. *Spine* **2004**, *29*, 2691–2699. [CrossRef] [PubMed]
4. Little, J.P.; Pearcy, M.J.; Tevelen, G.; Evans, J.H.; Pettet, G.; Adam, C.J. The mechanical response of the ovine lumbar anulus fibrosus to uniaxial, biaxial and shear loads. *J. Mech. Behav. Biomed. Mater.* **2010**, *3*, 146–157. [CrossRef] [PubMed]
5. Roughley, P.J.; Alini, M.; Antoniou, J. The role of proteoglycans in aging, degeneration and repair of the intervertebral disc. *Biochem. Soc. Trans.* **2002**, *30*, 869–874. [CrossRef] [PubMed]
6. Melrose, J.; Whitelock, J.M. Chapter 467 Extracellular matrix. In *Wiley Encyclopedia of Biomedical Engineering*; Akay, M., Ed.; John Wiley and Son Inc.: Hoboken, NJ, USA, 1999.
7. Iozzo, R.V.; Murdoch, A.D. Proteoglycans of the extracellular environment: Clues from the gene and protein side offer novel perspectives in molecular diversity and function. *FASEB J.* **1996**, *10*, 598–614. [PubMed]
8. Roughley, P.J.; Melching, L.I.; Heathfield, T.F.; Pearce, R.H.; Mort, J.S. The structure and degradation of aggrecan in human intervertebral disc. *Eur. Spine J.* **2006**, *15* (Suppl. S3), S326–S332. [CrossRef] [PubMed]
9. Hardingham, T. Cartilage: Aggrecan-link protein-hyaluronan aggregates. In *Glycoforum: Hyaluronan Today*; Mizutani Foundation for Glycoscience: Tokyo, Japan, 1998.
10. Eyre, D.R. Biochemistry of the intervertebral disc. *Int. Rev. Connect. Tissue Res.* **1979**, *8*, 227–291. [PubMed]
11. Eyre, D.R.; Muir, H. Types I and II collagens in intervertebral disc. Interchanging radial distributions in annulus fibrosus. *Biochem. J.* **1976**, *157*, 267–270. [CrossRef] [PubMed]
12. Brown, S.; Melrose, J.; Caterson, B.; Roughley, P.; Eisenstein, S.M.; Roberts, S. A comparative evaluation of the small leucine-rich proteoglycans of pathological human intervertebral discs. *Eur. Spine J.* **2012**, *21* (Suppl. S2), S154–S159. [CrossRef] [PubMed]
13. Melrose, J.; Fuller, E.S.; Roughley, P.J.; Smith, M.M.; Kerr, B.; Hughes, C.E.; Caterson, B.; Little, C.B. Fragmentation of decorin, biglycan, lumican and keratocan is elevated in degenerate human meniscus, knee and hip articular cartilages compared with age-matched macroscopically normal and control tissues. *Arthritis Res. Ther.* **2008**, *10*, R79. [CrossRef] [PubMed]
14. Hayes, A.J.; Shu, C.C.; Lord, M.S.; Little, C.B.; Whitelock, J.M.; Melrose, J. Pericellular colocalisation and interactive properties of type VI collagen and perlecan in the intervertebral disc. *Eur. Cell Mater.* **2016**, *32*, 40–57. [CrossRef] [PubMed]
15. Melrose, J.; Roughley, P.J. Proteoglycans of the intervertebral disc. In *The Intervertebral Disc Molecular and Structural Studies of the Disc in Health and Disease*; Shapiro, I., Risbud, M.V., Eds.; Springer: Vienna, Austria, 2014; pp. 53–78.
16. Stanton, H.; Melrose, J.; Little, C.B.; Fosang, A.J. Proteoglycan degradation by the ADAMTS family of proteinases. *Biochim. Biophys. Acta* **2011**, *1812*, 1616–1629. [CrossRef] [PubMed]
17. Richardson, S.; Freemont, A.J.; Hoyland, J.A. Pathogenesis of Intervertebral disc degeneration. In *The Intervertebral Disc Molecular and Structural Studies of the Disc in Health and Disease*; Shapiro, I., Risbud, M.V., Eds.; Springer: Vienna, Austria, 2014; pp. 177–200.
18. Richardson, S.M.; Doyle, P.; Minogue, B.M.; Gnanalingham, K.; Hoyland, J.A. Increased expression of matrix metalloproteinase-10, nerve growth factor and substance P in the painful degenerate intervertebral disc. *Arthritis Res. Ther.* **2009**, *11*, R126. [CrossRef] [PubMed]
19. Wang, W.J.; Yu, X.H.; Wang, C.; Yang, W.; He, W.S.; Zhang, S.J.; Yan, Y.G.; Zhang, J. MMPs and ADAMTSs in intervertebral disc degeneration. *Clin. Chim. Acta* **2015**, *448*, 238–246. [CrossRef] [PubMed]

20. Blain, E.J. Mechanical regulation of matrix metalloproteinases. *Front. Biosci.* **2007**, *12*, 507–527. [CrossRef] [PubMed]
21. Melrose, J.; Smith, S.M.; Little, C.B.; Moore, R.J.; Vernon-Roberts, B.; Fraser, R.D. Recent advances in annular pathobiology provide insights into rim-lesion mediated intervertebral disc degeneration and potential new approaches to annular repair strategies. *Eur. Spine J.* **2008**, *17*, 1131–1148. [CrossRef] [PubMed]
22. Adams, M.A.; Roughley, P.J. What is intervertebral disc degeneration, and what causes it? *Spine* **2006**, *31*, 2151–2161. [CrossRef] [PubMed]
23. Johnson, W.E.; Caterson, B.; Eisenstein, S.M.; Hynds, D.L.; Snow, D.M.; Roberts, S. Human intervertebral disc aggrecan inhibits nerve growth in vitro. *Arthritis Rheum.* **2002**, *46*, 2658–2664. [CrossRef] [PubMed]
24. Johnson, W.E.; Caterson, B.; Eisenstein, S.M.; Roberts, S. Human intervertebral disc aggrecan inhibits endothelial cell adhesion and cell migration in vitro. *Spine* **2005**, *30*, 1139–1147. [CrossRef] [PubMed]
25. Andersson, G. The Epidemiology of Spinal Disorders. In *The Adult Spine: Principles and Practice*; Lippincott-Raven: Philadelphia, PA, USA, 1997; pp. 93–141.
26. Melrose, J. Strategies in regenerative medicine for intervertebral disc repair using mesenchymal stem cells and bioscaffolds. *Regen. Med.* **2016**, *11*, 705–724. [CrossRef] [PubMed]
27. Maidhof, R.; Alipui, D.O.; Rafiuddin, A.; Levine, M.; Grande, D.A.; Chahine, N.O. Emerging trends in biological therapy for intervertebral disc degeneration. *Discov. Med.* **2012**, *14*, 401–411. [PubMed]
28. Than, K.D.; Rahman, S.U.; Wang, L.; Khan, A.; Kyere, K.A.; Than, T.T.; Miyata, Y.; Park, Y.S.; La Marca, F.; Kim, H.M.; et al. Intradiscal injection of simvastatin results in radiologic, histologic, and genetic evidence of disc regeneration in a rat model of degenerative disc disease. *Spine J.* **2014**, *14*, 1017–1028. [CrossRef] [PubMed]
29. Wuertz, K.; Quero, L.; Sekiguchi, M.; Klawitter, M.; Nerlich, A.; Konno, S.; Kikuchi, S.; Boos, N. The red wine polyphenol resveratrol shows promising potential for the treatment of nucleus pulposus-mediated pain in vitro and in vivo. *Spine* **2011**, *36*, E1373–E1384. [CrossRef] [PubMed]
30. Anderson, D.G.; Tannoury, C. Molecular pathogenic factors in symptomatic disc degeneration. *Spine J.* **2005**, *5*, 260S–266S. [CrossRef] [PubMed]
31. Fuller, E.S.; Shu, C.; Smith, M.M.; Little, C.B.; Melrose, J. Hyaluronan oligosaccharides stimulate MMP and anabolic gene expression in vitro by intervertebral disc cells and annular repair in vivo. *J. Tissue Eng. Regen. Med.* **2016**. [CrossRef]
32. Gawri, R.; Antoniou, J.; Ouellet, J.; Awwad, W.; Steffen, T.; Roughley, P.; Haglund, L.; Mwale, F. Best paper NASS 2013: Link-N can stimulate proteoglycan synthesis in the degenerated human intervertebral discs. *Eur. Cell Mater.* **2013**, *26*, 107–119. [CrossRef] [PubMed]
33. Mwale, F.; Masuda, K.; Pichika, R.; Epure, L.M.; Yoshikawa, T.; Hemmad, A.; Roughley, P.J.; Antoniou, J. The efficacy of Link N as a mediator of repair in a rabbit model of intervertebral disc degeneration. *Arthritis Res. Ther.* **2011**, *13*, R120. [CrossRef] [PubMed]
34. Petit, A.; Yao, G.; Rowas, S.A.; Gawri, R.; Epure, L.; Antoniou, J.; Mwale, F. Effect of synthetic link N peptide on the expression of type I and type II collagens in human intervertebral disc cells. *Tissue Eng. Part A* **2011**, *17*, 899–904. [CrossRef] [PubMed]
35. Mwale, F.; Demers, C.N.; Petit, A.; Roughley, P.; Poole, A.R.; Steffen, T.; Aebi, M.; Antoniou, J. A synthetic peptide of link protein stimulates the biosynthesis of collagens II, IX and proteoglycan by cells of the intervertebral disc. *J. Cell. Biochem.* **2003**, *88*, 1202–1213. [CrossRef] [PubMed]
36. Antoniou, J.; Wang, H.T.; Alaseem, A.M.; Haglund, L.; Roughley, P.J.; Mwale, F. The effect of Link N on differentiation of human bone marrow-derived mesenchymal stem cells. *Arthritis Res. Ther.* **2012**, *14*, R267. [CrossRef] [PubMed]
37. Mwale, F.; Wang, H.T.; Roughley, P.; Antoniou, J.; Haglund, L. Link N and mesenchymal stem cells can induce regeneration of the early degenerate Intervertebral Disc. *Tissue Eng. Part A* **2014**. [CrossRef] [PubMed]
38. Kwon, Y.J.; Lee, J.W.; Moon, E.J.; Chung, Y.G.; Kim, O.S.; Kim, H.J. Anabolic effects of Peniel 2000, a peptide that regulates TGF-β1 signaling on intervertebral disc degeneration. *Spine* **2013**, *38*, E49–E58. [CrossRef] [PubMed]
39. Kwon, Y.J. Resveratrol has anabolic effects on disc degeneration in a rabbit model. *J. Korean Med. Sci.* **2013**, *28*, 939–945. [CrossRef] [PubMed]
40. Li, X.; Phillips, F.M.; An, H.S.; Ellman, M.; Thonar, E.J.; Wu, W.; Park, D.; Im, H.J. The action of resveratrol, a phytoestrogen found in grapes, on the intervertebral disc. *Spine* **2008**, *33*, 2586–2595. [CrossRef] [PubMed]

41. Zhang, H.; Lin, C.Y. Simvastatin stimulates chondrogenic phenotype of intervertebral disc cells partially through BMP-2 pathway. *Spine* **2008**, *33*, E525–E531. [CrossRef] [PubMed]
42. Zhang, H.; Wang, L.; Park, J.B.; Park, P.; Yang, V.C.; Hollister, S.J.; La Marca, F.; Lin, C.Y. Intradiscal injection of simvastatin retards progression of intervertebral disc degeneration induced by stab injury. *Arthritis Res. Ther.* **2009**, *11*, R172. [CrossRef] [PubMed]
43. Gologorsky, Y.; Chi, J. Statins for disc degeneration. *Neurosurgery* **2014**, *74*, N18–N19. [CrossRef] [PubMed]
44. Hu, M.H.; Yang, K.C.; Chen, Y.J.; Sun, Y.H.; Yang, S.H. Lovastatin prevents discography-associated degeneration and maintains the functional morphology of intervertebral discs. *Spine J.* **2014**, *14*, 2459–2466. [CrossRef] [PubMed]
45. Karamouzian, S.; Eskandary, H.; Saeed, A.; Reihani-Kermani, H.; Aboosaeedi, H.R.; Malekpoor-Afshar, R.; Safizade, H.; Eskandari, M. Effect of atorvastatin on angiogenesis in degenerated intervertebral disc in rat. *Spine* **2011**, *36*, 1824–1828. [CrossRef] [PubMed]
46. Wong, R.W.; Rabie, B.; Bendeus, M.; Hagg, U. The effects of Rhizoma Curculiginis and Rhizoma Drynariae extracts on bones. *Chin. Med.* **2007**, *2*, 13. [CrossRef] [PubMed]
47. Alam, M.A.; Subhan, N.; Rahman, M.M.; Uddin, S.J.; Reza, H.M.; Sarker, S.D. Effect of citrus flavonoids, naringin and naringenin, on metabolic syndrome and their mechanisms of action. *Adv. Nutr.* **2014**, *5*, 404–417. [CrossRef] [PubMed]
48. Li, N.; Whitaker, C.; Xu, Z.; Heggeness, M.; Yang, S.Y. Therapeutic effects of naringin on degenerative human nucleus pulposus cells for discogenic low back pain. *Spine J.* **2016**, *16*, 1231–1237. [CrossRef] [PubMed]
49. Freeman, B.J.; Kuliwaba, J.S.; Jones, C.F.; Shu, C.C.; Colloca, C.J.; Zarrinkalam, M.R.; Mulaibrahimovic, A.; Gronthos, S.; Zannettino, A.C.; Howell, S. Allogeneic mesenchymal precursor cells promote healing in postero-lateral annular lesions and improve indices of lumbar intervertebral disc degeneration in an ovine model. *Spine* **2016**, *41*, 1331–1339. [CrossRef] [PubMed]
50. Pettine, K.; Suzuki, R.; Sand, T.; Murphy, M. Treatment of discogenic back pain with autologous bone marrow concentrate injection with minimum two year follow-up. *Int. Orthop.* **2016**, *40*, 135–140. [CrossRef] [PubMed]
51. Sakai, D.; Andersson, G.B. Stem cell therapy for intervertebral disc regeneration: Obstacles and solutions. *Nat. Rev. Rheumatol.* **2015**, *11*, 243–256. [CrossRef] [PubMed]
52. Zeckser, J.; Wolff, M.; Tucker, J.; Goodwin, J. Multipotent mesenchymal stem cell treatment for discogenic low back pain and disc degeneration. *Stem Cells Int.* **2016**, *2016*, 3908389. [CrossRef] [PubMed]
53. Crevensten, G.; Walsh, A.J.; Ananthakrishnan, D.; Page, P.; Wahba, G.M.; Lotz, J.C.; Berven, S. Intervertebral disc cell therapy for regeneration: Mesenchymal stem cell implantation in rat intervertebral discs. *Ann. Biomed. Eng.* **2004**, *32*, 430–434. [CrossRef] [PubMed]
54. Vadala, G.; Sowa, G.; Hubert, M.; Gilbertson, L.G.; Denaro, V.; Kang, J.D. Mesenchymal stem cells injection in degenerated intervertebral disc: Cell leakage may induce osteophyte formation. *J. Tissue Eng. Regen. Med.* **2012**, *6*, 348–355. [CrossRef] [PubMed]
55. Longo, U.G.; Papapietro, N.; Petrillo, S.; Franceschetti, E.; Maffulli, N.; Denaro, V. Mesenchymal stem cell for prevention and management of intervertebral disc degeneration. *Stem Cells Int.* **2012**, *2012*, 921053. [CrossRef] [PubMed]
56. Oehme, D.; Goldschlager, T.; Ghosh, P.; Rosenfeld, J.V.; Jenkin, G. Cell-based therapies used to treat lumbar degenerative disc disease: A systematic review of animal studies and human clinical trials. *Stem Cells Int.* **2015**, *2015*, 946031. [CrossRef] [PubMed]
57. Oehme, D.; Goldschlager, T.; Rosenfeld, J.V.; Ghosh, P.; Jenkin, G. The role of stem cell therapies in degenerative lumbar spine disease: A review. *Neurosurg. Rev.* **2015**, *38*, 429–445. [CrossRef] [PubMed]
58. Richardson, S.M.; Hoyland, J.A.; Mobasheri, R.; Csaki, C.; Shakibaei, M.; Mobasheri, A. Mesenchymal stem cells in regenerative medicine: Opportunities and challenges for articular cartilage and intervertebral disc tissue engineering. *J. Cell. Physiol.* **2010**, *222*, 23–32. [CrossRef] [PubMed]
59. Krock, E.; Rosenzweig, D.H.; Haglund, L. The inflammatory milieu of the degenerate disc: Is mesenchymal stem cell-based therapy for intervertebral disc repair a feasible approach? *Curr. Stem Cell Res. Ther.* **2015**, *10*, 317–328. [CrossRef] [PubMed]
60. Melrose, J. The promise of mesenchymal stem cells for intervertebral disc repair. *J. Stem Cell Res. Ther.* **2017**, *2*, 61–64.

61. Shim, E.K.; Lee, J.S.; Kim, D.E.; Kim, S.K.; Jung, B.J.; Choi, E.Y.; Kim, C.S. Autogenous mesenchymal stem cells from the vertebral body enhance intervertebral disc regeneration by paracrine interaction: An in vitro pilot study. *Cell Transplant.* **2016**. [CrossRef] [PubMed]
62. An, H.S.; Thonar, E.J.; Masuda, K. Biological repair of intervertebral disc. *Spine* **2003**, *28*, S86–S92. [CrossRef] [PubMed]
63. Masuda, K. Biological repair of the degenerated intervertebral disc by the injection of growth factors. *Eur. Spine J.* **2008**, *17* (Suppl. S4), 441–451. [CrossRef] [PubMed]
64. Meisel, H.J.; Siodla, V.; Ganey, T.; Minkus, Y.; Hutton, W.C.; Alasevic, O.J. Clinical experience in cell-based therapeutics: Disc chondrocyte transplantation A treatment for degenerated or damaged intervertebral disc. *Biomol. Eng.* **2007**, *24*, 5–21. [CrossRef] [PubMed]
65. Orozco, L.; Soler, R.; Morera, C.; Alberca, M.; Sanchez, A.; Garcia-Sancho, J. Intervertebral disc repair by autologous mesenchymal bone marrow cells: A pilot study. *Transplantation* **2011**, *92*, 822–828. [CrossRef] [PubMed]
66. Yoshikawa, T.; Ueda, Y.; Miyazaki, K.; Koizumi, M.; Takakura, Y. Disc regeneration therapy using marrow mesenchymal cell transplantation: A report of two case studies. *Spine* **2010**, *35*, E475–E480. [CrossRef] [PubMed]
67. Bae, H.W.; Amirdelfan, K.; Coric, D.; McJunkin, T.L.; Pettine, K.A.; Hong, H.J.; DePalma, M.J.; Kim, K.D.; Beckworth, W.J.; et al. A phase II study demonstrating efficacy and safety of mesenchymal precursor cells in low back pain due to disc degeneration. *Spine J.* **2014**, *14*, S31–S32. [CrossRef]
68. Alini, M.; Eisenstein, S.M.; Ito, K.; Little, C.; Kettler, A.A.; Masuda, K.; Melrose, J.; Ralphs, J.; Stokes, I.; Wilke, H.J. Are animal models useful for studying human disc disorders/degeneration? *Eur. Spine J.* **2008**, *17*, 2–19. [CrossRef] [PubMed]
69. Daly, C.; Ghosh, P.; Jenkin, G.; Oehme, D.; Goldschlager, T. A Review of Animal Models of Intervertebral Disc Degeneration: Pathophysiology, Regeneration, and Translation to the Clinic. *BioMed Res. Int.* **2016**, *2016*, 5952165. [CrossRef] [PubMed]
70. Melrose, J.; Shu, C.; Young, C.; Ho, R.; Smith, M.M.; Young, A.A.; Smith, S.S.; Gooden, B.; Dart, A.; Podadera, J.; et al. Mechanical destabilization induced by controlled annular incision of the intervertebral disc dysregulates metalloproteinase expression and induces disc degeneration. *Spine* **2012**, *37*, 18–25. [CrossRef] [PubMed]
71. Osti, O.L.; Vernon-Roberts, B.; Fraser, R.D. 1990 Volvo Award in experimental studies. Anulus tears and intervertebral disc degeneration. An experimental study using an animal model. *Spine* **1990**, *15*, 762–767. [PubMed]
72. Melrose, J.; Ghosh, P.; Taylor, T.K.; Hall, A.; Osti, O.L.; Vernon-Roberts, B.; Fraser, R.D. A longitudinal study of the matrix changes induced in the intervertebral disc by surgical damage to the annulus fibrosus. *J. Orthop. Res.* **1992**, *10*, 665–676. [CrossRef] [PubMed]
73. Detiger, S.E.; Hoogendoorn, R.J.; van der Veen, A.J.; van Royen, B.J.; Helder, M.N.; Koenderink, G.H.; Smit, T.H. Biomechanical and rheological characterization of mild intervertebral disc degeneration in a large animal model. *J. Orthop. Res.* **2013**, *31*, 703–709. [CrossRef] [PubMed]
74. Hoogendoorn, R.J.; Wuisman, P.I.; Smit, T.H.; Everts, V.E.; Helder, M.N. Experimental intervertebral disc degeneration induced by chondroitinase ABC in the goat. *Spine* **2007**, *32*, 1816–1825. [CrossRef] [PubMed]
75. Zhang, Y.; Drapeau, S.; An, H.S.; Markova, D.; Lenart, B.A.; Anderson, D.G. Histological features of the degenerating intervertebral disc in a goat disc-injury model. *Spine* **2011**, *36*, 1519–1527. [CrossRef] [PubMed]
76. Bergknut, N.; Meij, B.P.; Hagman, R.; de Nies, K.S.; Rutges, J.P.; Smolders, L.A.; Creemers, L.B.; Lagerstedt, A.S.; Hazewinkel, H.A.; Grinwis, G.C. Intervertebral disc disease in dogs—Part 1: A new histological grading scheme for classification of intervertebral disc degeneration in dogs. *Vet. J.* **2013**, *195*, 156–163. [CrossRef] [PubMed]
77. Bergknut, N.; Rutges, J.P.; Kranenburg, H.J.; Smolders, L.A.; Hagman, R.; Smidt, H.J.; Lagerstedt, A.S.; Penning, L.C.; Voorhout, G.; Hazewinkel, H.A.; et al. The dog as an animal model for intervertebral disc degeneration? *Spine* **2012**, *37*, 351–358. [CrossRef] [PubMed]
78. Seiler, G.; Hani, H.; Scheidegger, J.; Busato, A.; Lang, J. Staging of lumbar intervertebral disc degeneration in nonchondrodystrophic dogs using low-field magnetic resonance imaging. *Vet. Radiol. Ultrasound* **2003**, *44*, 179–184. [CrossRef] [PubMed]

79. Omlor, G.W.; Nerlich, A.G.; Wilke, H.J.; Pfeiffer, M.; Lorenz, H.; Schaaf-Keim, M.; Bertram, H.; Richter, W.; Carstens, C.; Guehring, T. A new porcine in vivo animal model of disc degeneration: Response of anulus fibrosus cells, chondrocyte-like nucleus pulposus cells, and notochordal nucleus pulposus cells to partial nucleotomy. *Spine* **2009**, *34*, 2730–2739. [CrossRef] [PubMed]
80. Chiang, C.J.; Cheng, C.K.; Sun, J.S.; Liao, C.J.; Wang, Y.H.; Tsuang, Y.H. The effect of a new anular repair after discectomy in intervertebral disc degeneration: An experimental study using a porcine spine model. *Spine* **2011**, *36*, 761–769. [CrossRef] [PubMed]
81. Kaigle, A.M.; Holm, S.H.; Hansson, T.H. 1997 Volvo Award winner in biomechanical studies. Kinematic behavior of the porcine lumbar spine: A chronic lesion model. *Spine* **1997**, *22*, 2796–2806. [CrossRef] [PubMed]
82. Moore, R.J.; Osti, O.L.; Vernon-Roberts, B.; Fraser, R.D. Changes in endplate vascularity after an outer anulus tear in the sheep. *Spine* **1992**, *17*, 874–878. [CrossRef] [PubMed]
83. Moore, R.J.; Crotti, T.N.; Osti, O.L.; Fraser, R.D.; Vernon-Roberts, B. Osteoarthrosis of the facet joints resulting from anular rim lesions in sheep lumbar discs. *Spine* **1999**, *24*, 519–525. [CrossRef] [PubMed]
84. Moore, R.J.; Vernon-Roberts, B.; Osti, O.L.; Fraser, R.D. Remodeling of vertebral bone after outer anular injury in sheep. *Spine* **1996**, *21*, 936–940. [CrossRef] [PubMed]
85. Melrose, J.; Roberts, S.; Smith, S.; Menage, J.; Ghosh, P. Increased nerve and blood vessel ingrowth associated with proteoglycan depletion in an ovine anular lesion model of experimental disc degeneration. *Spine* **2002**, *27*, 1278–1285. [CrossRef] [PubMed]
86. Melrose, J.; Smith, S.; Little, C.B.; Kitson, J.; Hwa, S.Y.; Ghosh, P. Spatial and temporal localization of transforming growth factor-beta, fibroblast growth factor-2, and osteonectin, and identification of cells expressing alpha-smooth muscle actin in the injured anulus fibrosus: Implications for extracellular matrix repair. *Spine* **2002**, *27*, 1756–1764. [CrossRef] [PubMed]
87. Osti, O.L.; Vernon-Roberts, B.; Moore, R.; Fraser, R.D. Annular tears and disc degeneration in the lumbar spine. A post-mortem study of 135 discs. *J. Bone Jt. Surg. Br.* **1992**, *74*, 678–682.
88. De Visser, H.; Rowe, C.; Pearcy, M. A robotic testing facility for the measurement of the mechanics of spinal joints. *Proc. Inst. Mech. Eng. H* **2007**, *221*, 221–227. [CrossRef] [PubMed]
89. Thompson, R.E.; Pearcy, M.J.; Downing, K.J.; Manthey, B.A.; Parkinson, I.H.; Fazzalari, N.L. Disc lesions and the mechanics of the intervertebral joint complex. *Spine* **2000**, *25*, 3026–3035. [CrossRef] [PubMed]
90. Hilton, R.C.; Ball, J. Vertebral rim lesions in the dorsolumbar spine. *Ann. Rheum. Dis.* **1984**, *43*, 302–307. [CrossRef] [PubMed]
91. Melrose, J. A global pictorial assessment of the intervertebral disc cell in several species reveals a remarkable biodiversity in this cell type which should be taken into account in experimental studies on intervertebral disc repair. *Spine Res.* **2016**, *2*, 1.
92. Fagan, A.; Moore, R.; Vernon Roberts, B.; Blumbergs, P.; Fraser, R. ISSLS prize winner: The innervation of the intervertebral disc: A quantitative analysis. *Spine* **2003**, *28*, 2570–2576. [CrossRef] [PubMed]
93. Vos, T.; Flaxman, A.D.; Naghavi, M.; Lozano, R.; Michaud, C.; Ezzati, M.; Shibuya, K.; Salomon, J.A.; Abdalla, S.; Aboyans, V.; et al. Years lived with disability (YLDs) for 1160 sequelae of 289 diseases and injuries 1990–2010: A systematic analysis for the Global Burden of Disease Study 2010. *Lancet* **2012**, *380*, 2163–2196. [CrossRef]
94. Maniadakis, N.; Gray, A. The economic burden of back pain in the UK. *Pain* **2000**, *84*, 95–103. [CrossRef]
95. Walker, B.F.; Muller, R.; Grant, W.D. Low back pain in Australian adults: The economic burden. *Asia Pac. J. Public Health* **2003**, *15*, 79–87. [CrossRef] [PubMed]
96. Briggs, A.M.; Buchbinder, R. Back pain: A national health priority area in australia? *Med. J. Aust.* **2009**, *190*, 499–502. [PubMed]
97. Ehrlich, G.E.; Khaltaev, N.G.; Chronic Respiratory Diseases and Arthritis Team. *Low Back Pain Initiative*; World Health Organization: Geneva, Switzerland, 1999; p. 152.
98. Walker, B.F.; Muller, R.; Grant, W.D. Low back pain in Australian adults: Prevalence and associated disability. *J. Manip. Physiol. Ther.* **2004**, *27*, 238–244. [CrossRef] [PubMed]
99. Hoy, D.; March, L.; Brooks, P.; Blyth, F.; Woolf, A.; Bain, C.; Williams, G.; Smith, E.; Vos, T.; Barendregt, J.; et al. The global burden of low back pain: Estimates from the Global Burden of Disease 2010 study. *Ann. Rheum. Dis.* **2014**, *73*, 968–974. [CrossRef] [PubMed]

100. Hoy, D.; March, L.; Brooks, P.; Woolf, A.; Blyth, F.; Vos, T.; Buchbinder, R. Measuring the global burden of low back pain. *Best Pract. Res. Clin. Rheumatol.* **2010**, *24*, 155–165. [CrossRef] [PubMed]
101. Hoy, D.G.; Smith, E.; Cross, M.; Sanchez-Riera, L.; Buchbinder, R.; Blyth, F.M.; Brooks, P.; Woolf, A.D.; Osborne, R.H.; Fransen, M.; et al. The global burden of musculoskeletal conditions for 2010: An overview of methods. *Ann. Rheum. Dis.* **2014**, *73*, 982–989. [CrossRef] [PubMed]
102. Ho, G.; Leung, V.Y.; Cheung, K.M.; Chan, D. Effect of severity of intervertebral disc injury on mesenchymal stem cell-based regeneration. *Connect. Tissue Res.* **2008**, *49*, 15–21. [CrossRef] [PubMed]
103. Jeong, J.H.; Jin, E.S.; Min, J.K.; Jeon, S.R.; Park, C.S.; Kim, H.S.; Choi, K.H. Human mesenchymal stem cells implantation into the degenerated coccygeal disc of the rat. *Cytotechnology* **2009**, *59*, 55–64. [CrossRef] [PubMed]
104. Leung, V.Y.; Aladin, D.M.; Lv, F.; Tam, V.; Sun, Y.; Lau, R.Y.; Hung, S.C.; Ngan, A.H.; Tang, B.; Lim, C.T.; et al. Mesenchymal stem cells reduce intervertebral disc fibrosis and facilitate repair. *Stem Cells* **2014**, *32*, 2164–2177. [CrossRef] [PubMed]
105. Yang, F.; Leung, V.Y.; Luk, K.D.; Chan, D.; Cheung, K.M. Mesenchymal stem cells arrest intervertebral disc degeneration through chondrocytic differentiation and stimulation of endogenous cells. *Mol. Ther.* **2009**, *17*, 1959–1966. [CrossRef] [PubMed]
106. Cheung, K.M.; Karppinen, J.; Chan, D.; Ho, D.W.; Song, Y.Q.; Sham, P.; Cheah, K.S.; Leong, J.C.; Luk, K.D. Prevalence and pattern of lumbar magnetic resonance imaging changes in a population study of one thousand forty-three individuals. *Spine* **2009**, *34*, 934–940. [CrossRef] [PubMed]
107. Livshits, G.; Popham, M.; Malkin, I.; Sambrook, P.N.; Macgregor, A.J.; Spector, T.; Williams, F.M. Lumbar disc degeneration and genetic factors are the main risk factors for low back pain in women: The UK Twin Spine Study. *Ann. Rheum. Dis.* **2011**, *70*, 1740–1745. [CrossRef] [PubMed]
108. Bogduk, N. The lumbar disc and low back pain. *Neurosurg. Clin. N. Am.* **1991**, *2*, 791–806. [PubMed]
109. Freemont, A.J. The cellular pathobiology of the degenerate intervertebral disc and discogenic back pain. *Rheumatology* **2009**, *48*, 5–10. [CrossRef] [PubMed]
110. Freemont, A.J.; Peacock, T.E.; Goupille, P.; Hoyland, J.A.; O'Brien, J.; Jayson, M.I. Nerve ingrowth into diseased intervertebral disc in chronic back pain. *Lancet* **1997**, *350*, 178–181. [CrossRef]
111. Ahn, S.H.; Cho, Y.W.; Ahn, M.W.; Jang, S.H.; Sohn, Y.K.; Kim, H.S. mRNA expression of cytokines and chemokines in herniated lumbar intervertebral discs. *Spine* **2002**, *27*, 911–917. [CrossRef] [PubMed]
112. Friberg, S.; Hirsch, C. Anatomical and clinical studies on lumbar disc degeneration. *Clin. Orthop. Relat. Res.* **1992**, *19*, 222–242. [CrossRef]
113. Battie, M.C.; Videman, T.; Levalahti, E.; Gill, K.; Kaprio, J. Heritability of low back pain and the role of disc degeneration. *Pain* **2007**, *131*, 272–280. [CrossRef] [PubMed]
114. Leung, V.Y.; Chan, D.; Cheung, K.M. Regeneration of intervertebral disc by mesenchymal stem cells: Potentials, limitations, and future direction. *Eur. Spine J.* **2006**, *15* (Suppl. S3), S406–S413. [CrossRef] [PubMed]
115. Zhang, Y.; Chee, A.; Thonar, E.J.; An, H.S. Intervertebral disk repair by protein, gene, or cell injection: A framework for rehabilitation-focused biologics in the spine. *PM R* **2011**, *3*, S88–S94. [CrossRef] [PubMed]
116. Guterl, C.C.; See, E.Y.; Blanquer, S.B.; Pandit, A.; Ferguson, S.J.; Benneker, L.M.; Grijpma, D.W.; Sakai, D.; Eglin, D.; Alini, M.; et al. Challenges and strategies in the repair of ruptured annulus fibrosus. *Eur. Cell Mater.* **2013**, *25*, 1–21. [CrossRef] [PubMed]
117. Hegewald, A.A.; Zouhair, S.; Endres, M.; Cabraja, M.; Woiciechowsky, C.; Thome, C.; Kaps, C. Towards biological anulus repair: TGF-β3, FGF-2 and human serum support matrix formation by human anulus fibrosus cells. *Tissue Cell* **2013**, *45*, 68–76. [CrossRef] [PubMed]
118. Vernengo, J.; Fussell, G.W.; Smith, N.G.; Lowman, A.M. Synthesis and characterization of injectable bioadhesive hydrogels for nucleus pulposus replacement and repair of the damaged intervertebral disc. *J. Biomed. Mater. Res. B Appl. Biomater.* **2010**, *93*, 309–317. [CrossRef] [PubMed]
119. Bergknut, N.; Grinwis, G.; Pickee, E.; Auriemma, E.; Lagerstedt, A.S.; Hagman, R.; Hazewinkel, H.A.; Meij, B.P. Reliability of macroscopic grading of intervertebral disk degeneration in dogs by use of the Thompson system and comparison with low-field magnetic resonance imaging findings. *Am. J. Vet. Res.* **2011**, *72*, 899–904. [CrossRef] [PubMed]
120. Hodges, P.W.; Galea, M.P.; Holm, S.; Holm, A.K. Corticomotor excitability of back muscles is affected by intervertebral disc lesion in pigs. *Eur. J. Neurosci.* **2009**, *29*, 1490–1500. [CrossRef] [PubMed]

121. Colloca, C.J.; Gunzburg, R.; Freeman, B.J.; Szpalski, M.; Afifi, M.; Moore, R.J. Biomechancial quantification of pathologic manipulable spinal lesions: An in vivo ovine model of spondylolysis and intervertebral disc degeneration. *J. Manip. Physiol. Ther.* **2012**, *35*, 354–366. [CrossRef] [PubMed]
122. Colloca, C.J.; Keller, T.S.; Harrison, D.E.; Moore, R.J.; Gunzburg, R.; Harrison, D.D. Spinal manipulation force and duration affect vertebral movement and neuromuscular responses. *Clin. Biomech.* **2006**, *21*, 254–262. [CrossRef] [PubMed]
123. Colloca, C.J.; Keller, T.S.; Moore, R.J.; Gunzburg, R.; Harrison, D.E. Intervertebral disc degeneration reduces vertebral motion responses. *Spine* **2007**, *32*, E544–E550. [CrossRef] [PubMed]
124. Colloca, C.J.; Keller, T.S.; Moore, R.J.; Gunzburg, R.; Harrison, D.E. Effects of disc degeneration on neurophysiological responses during dorsoventral mechanical excitation of the ovine lumbar spine. *J. Electromyogr. Kinesiol.* **2008**, *18*, 829–837. [CrossRef] [PubMed]
125. Keller, T.S.; Colloca, C.J.; Moore, R.J.; Gunzburg, R.; Harrison, D.E.; Harrison, D.D. Three-dimensional vertebral motions produced by mechanical force spinal manipulation. *J. Manip. Physiol. Ther.* **2006**, *29*, 425–436. [CrossRef] [PubMed]
126. Hodges, P.; James, G.; Blomster, L.; Hall, L.; Schmid, A.; Shu, C.; Little, C.B.; Melrose, J. Multifidus muscle changes after back injury are characterized by structural remodeling of muscle, adipose and connective tissue, but not muscle atrophy: Molecular and morphological evidence. *Spine* **2015**, *40*, 1057–1071. [CrossRef] [PubMed]
127. Hodges, P.; Holm, A.K.; Hansson, T.; Holm, S. Rapid atrophy of the lumbar multifidus follows experimental disc or nerve root injury. *Spine* **2006**, *31*, 2926–2933. [CrossRef] [PubMed]
128. Hodges, P.W.; James, G.; Blomster, L.; Hall, L.; Schmid, A.B.; Shu, C.; Little, C.; Melrose, J. Can proinflammatory cytokine gene expression explain multifidus muscle fiber changes after an intervertebral disc lesion? *Spine* **2014**, *39*, 1010–1017. [CrossRef] [PubMed]
129. Freeman, M.D.; Woodham, M.A.; Woodham, A.W. The role of the lumbar multifidus in chronic low back pain: A review. *PM R* **2010**, *2*, 142–146. [CrossRef] [PubMed]
130. Holm, S.; Maroudas, A.; Urban, J.P.; Selstam, G.; Nachemson, A. Nutrition of the intervertebral disc: Solute transport and metabolism. *Connect. Tissue Res.* **1981**, *8*, 101–119. [CrossRef] [PubMed]
131. Bibby, S.R.; Urban, J.P. Effect of nutrient deprivation on the viability of intervertebral disc cells. *Eur. Spine J.* **2004**, *13*, 695–701. [CrossRef] [PubMed]
132. Holm, S.; Selstam, G. Oxygen tension alterations in the intervertebral disc as a response to changes in the arterial blood. *Ups. J. Med. Sci.* **1982**, *87*, 163–174. [CrossRef] [PubMed]
133. Horner, H.A.; Urban, J.P. 2001 Volvo Award Winner in Basic Science Studies: Effect of nutrient supply on the viability of cells from the nucleus pulposus of the intervertebral disc. *Spine* **2001**, *26*, 2543–2549. [CrossRef] [PubMed]
134. Urban, J.P.; Smith, S.; Fairbank, J.C. Nutrition of the intervertebral disc. *Spine* **2004**, *29*, 2700–2709. [CrossRef] [PubMed]
135. Diamant, B.; Karlsson, J.; Nachemson, A. Correlation between lactate levels and pH in discs of patients with lumbar rhizopathies. *Experientia* **1968**, *24*, 1195–1196. [CrossRef] [PubMed]
136. Razaq, S.; Wilkins, R.J.; Urban, J.P. The effect of extracellular pH on matrix turnover by cells of the bovine nucleus pulposus. *Eur. Spine J.* **2003**, *12*, 341–349. [CrossRef] [PubMed]
137. Ellman, M.B.; An, H.S.; Muddasani, P.; Im, H.J. Biological impact of the fibroblast growth factor family on articular cartilage and intervertebral disc homeostasis. *Gene* **2008**, *420*, 82–89. [CrossRef] [PubMed]
138. Kurakawa, T.; Kakutani, K.; Morita, Y.; Kato, Y.; Yurube, T.; Hirata, H.; Miyazaki, S.; Terashima, Y.; Maeno, K.; Takada, T.; et al. Functional impact of integrin α5β1 on the homeostasis of intervertebral discs: A study of mechanotransduction pathways using a novel dynamic loading organ culture system. *Spine J.* **2015**, *15*, 417–426. [CrossRef] [PubMed]
139. Pratsinis, H.; Kletsas, D. Growth factors in intervertebral disc homeostasis. *Connect. Tissue Res.* **2008**, *49*, 273–276. [CrossRef] [PubMed]
140. Nachemson, A. Intradiscal measurements of pH in patients with lumbar rhizopathies. *Acta Orthop. Scand.* **1969**, *40*, 23–42. [CrossRef] [PubMed]
141. Naqvi, S.M.; Buckley, C.T. Extracellular matrix production by nucleus pulposus and bone marrow stem cells in response to altered oxygen and glucose microenvironments. *J. Anat.* **2015**, *227*, 757–766. [CrossRef] [PubMed]

142. Naqvi, S.M.; Buckley, C.T. Bone marrow stem cells in response to intervertebral disc-like matrix acidity and oxygen concentration: Implications for cell-based regenerative therapy. *Spine* **2016**, *41*, 743–750. [CrossRef] [PubMed]
143. Wuertz, K.; Godburn, K.; Iatridis, J.C. MSC response to pH levels found in degenerating intervertebral discs. *Biochem. Biophys. Res. Commun.* **2009**, *379*, 824–829. [CrossRef] [PubMed]
144. Wuertz, K.; Godburn, K.; Neidlinger-Wilke, C.; Urban, J.; Iatridis, J.C. Behavior of mesenchymal stem cells in the chemical microenvironment of the intervertebral disc. *Spine* **2008**, *33*, 1843–1849. [CrossRef] [PubMed]
145. Schleich, C.; Muller-Lutz, A.; Eichner, M.; Schmitt, B.; Matuschke, F.; Bittersohl, B.; Zilkens, C.; Wittsack, H.J.; Antoch, G.; Miese, F. Glycosaminoglycan chemical exchange saturation transfer of lumbar intervertebral discs in healthy volunteers. *Spine* **2016**, *41*, 146–152. [CrossRef] [PubMed]
146. Schleich, C.; Muller-Lutz, A.; Matuschke, F.; Sewerin, P.; Sengewein, R.; Schmitt, B.; Ostendorf, B.; Wittsack, H.J.; Stanke, K.; Antoch, G.; et al. Glycosaminoglycan chemical exchange saturation transfer of lumbar intervertebral discs in patients with spondyloarthritis. *J. Magn. Reson. Imaging* **2015**, *42*, 1057–1063. [CrossRef] [PubMed]
147. Melrose, J.; Ghosh, P.; Taylor, T.K.; Latham, J.; Moore, R. Topographical variation in the catabolism of aggrecan in an ovine annular lesion model of experimental disc degeneration. *J. Spinal Disord.* **1997**, *10*, 55–67. [CrossRef] [PubMed]
148. Melrose, J.; Ghosh, P.; Taylor, T.K.; Vernon-Roberts, B.; Latham, J.; Moore, R. Elevated synthesis of biglycan and decorin in an ovine annular lesion model of experimental disc degeneration. *Eur. Spine J.* **1997**, *6*, 376–384. [CrossRef] [PubMed]
149. Melrose, J.; Smith, S.M.; Fuller, E.S.; Young, A.A.; Roughley, P.J.; Dart, A.; Little, C.B. Biglycan and fibromodulin fragmentation correlates with temporal and spatial annular remodelling in experimentally injured ovine intervertebral discs. *Eur. Spine J.* **2007**, *16*, 2193–2205. [CrossRef] [PubMed]
150. Schollum, M.L.; Appleyard, R.C.; Little, C.B.; Melrose, J. A detailed microscopic examination of alterations in normal anular structure induced by mechanical destabilization in an ovine model of disc degeneration. *Spine* **2010**, *35*, 1965–1973. [CrossRef] [PubMed]
151. Kettler, A.; Wilke, H.J. Review of existing grading systems for cervical or lumbar disc and facet joint degeneration. *Eur. Spine J.* **2006**, *15*, 705–718. [CrossRef] [PubMed]
152. Gunzburg, R.; Parkinson, R.; Moore, R.; Cantraine, F.; Hutton, W.; Vernon-Roberts, B.; Fraser, R. A cadaveric study comparing discography, magnetic resonance imaging, histology, and mechanical behavior of the human lumbar disc. *Spine* **1992**, *17*, 417–426. [CrossRef] [PubMed]
153. Tertti, M.; Paajanen, H.; Laato, M.; Aho, H.; Komu, M.; Kormano, M. Disc degeneration in magnetic resonance imaging. A comparative biochemical, histologic, and radiologic study in cadaver spines. *Spine* **1991**, *16*, 629–634. [CrossRef] [PubMed]
154. Gibson, M.J.; Buckley, J.; Mawhinney, R.; Mulholland, R.C.; Worthington, B.S. Magnetic resonance imaging and discography in the diagnosis of disc degeneration. A comparative study of 50 discs. *J. Bone Jt. Surg. Br.* **1986**, *68*, 369–373.
155. Schneiderman, G.; Flannigan, B.; Kingston, S.; Thomas, J.; Dillin, W.H.; Watkins, R.G. Magnetic resonance imaging in the diagnosis of disc degeneration: Correlation with discography. *Spine* **1987**, *12*, 276–281. [CrossRef] [PubMed]
156. Melhem, E.R.; Caruthers, S.D.; Jara, H. Cervical spine: Three-dimensional MR imaging with magnetization transfer prepulsed turbo field echo techniques. *Radiology* **1998**, *207*, 815–821. [CrossRef] [PubMed]
157. Rumboldt, Z.; Marotti, M. Magnetization transfer, HASTE, and FLAIR imaging. *Magn. Reson. Imaging Clin. N. Am.* **2003**, *11*, 471–492. [CrossRef]
158. Taso, M.; Girard, O.M.; Duhamel, G.; Le Troter, A.; Feiweier, T.; Guye, M.; Ranjeva, J.P.; Callot, V. Tract-specific and age-related variations of the spinal cord microstructure: A multi-parametric MRI study using diffusion tensor imaging (DTI) and inhomogeneous magnetization transfer (ihMT). *NMR Biomed.* **2016**, *29*, 817–832. [CrossRef] [PubMed]
159. Yoshioka, H.; Onaya, H.; Itai, Y.; Nishimura, H.; Matsumura, A.; Tsunoda, T.; Kandatsu, S.; Koga, M.; Yoshikawa, K.; Kato, H.; et al. Comparison between magnetization transfer contrast and fast spin-echo MR imaging of degenerative disease of the cervical spine at 0.3 T. *Magn. Reson. Imaging* **1997**, *15*, 37–45. [CrossRef]

160. Haneder, S.; Ong, M.M.; Budjan, J.M.; Schmidt, R.; Konstandin, S.; Morelli, J.N.; Schad, L.R.; Schoenberg, S.O.; Kerl, U.H. 23Na-magnetic resonance imaging of the human lumbar vertebral discs: In vivo measurements at 3.0 T in healthy volunteers and patients with low back pain. *Spine J.* **2014**, *14*, 1343–1350. [CrossRef] [PubMed]
161. Insko, E.K.; Clayton, D.B.; Elliott, M.A. In vivo sodium MR imaging of the intervertebral disk at 4 T. *Acad. Radiol.* **2002**, *9*, 800–804. [CrossRef]
162. Malzacher, M.; Kalayciyan, R.; Konstandin, S.; Haneder, S.; Schad, L.R. Sodium-23 MRI of whole spine at 3 Tesla using a 5-channel receive-only phased-array and a whole-body transmit resonator. *Z. Med. Phys.* **2016**, *26*, 95–100. [CrossRef] [PubMed]
163. Noebauer-Huhmann, I.M.; Juras, V.; Pfirrmann, C.W.; Szomolanyi, P.; Zbyn, S.; Messner, A.; Wimmer, J.; Weber, M.; Friedrich, K.M.; Stelzeneder, D.; et al. Sodium MR imaging of the lumbar intervertebral disk at 7 T: Correlation with T2 mapping and modified Pfirrmann score at 3 T–preliminary results. *Radiology* **2012**, *265*, 555–564. [CrossRef] [PubMed]
164. Solanky, B.S.; Riemer, F.; Golay, X.; Wheeler-Kingshott, C.A. Sodium quantification in the spinal cord at 3 T. *Magn. Reson. Med.* **2013**, *69*, 1201–1208. [CrossRef] [PubMed]
165. Wang, C.; McArdle, E.; Fenty, M.; Witschey, W.; Elliott, M.; Sochor, M.; Reddy, R.; Borthakur, A. Validation of sodium magnetic resonance imaging of intervertebral disc. *Spine* **2010**, *35*, 505–510. [CrossRef] [PubMed]
166. Antoniou, J.; Epure, L.M.; Michalek, A.J.; Grant, M.P.; Iatridis, J.C.; Mwale, F. Analysis of quantitative magnetic resonance imaging and biomechanical parameters on human discs with different grades of degeneration. *J. Magn. Reson. Imaging* **2013**, *38*, 1402–1414. [CrossRef] [PubMed]
167. Antoniou, J.; Pike, G.B.; Steffen, T.; Baramki, H.; Poole, A.R.; Aebi, M.; Alini, M. Quantitative magnetic resonance imaging in the assessment of degenerative disc disease. *Magn. Reson. Med.* **1998**, *40*, 900–907. [CrossRef] [PubMed]
168. Kellgren, J.H.; Lawrence, J.S. Radiological assessment of osteo-arthrosis. *Ann. Rheum. Dis.* **1957**, *16*, 494–502. [CrossRef] [PubMed]
169. Kirkaldy-Willis, W.H.; Wedge, J.H.; Yong-Hing, K.; Reilly, J. Pathology and pathogenesis of lumbar spondylosis and stenosis. *Spine* **1978**, *3*, 319–328. [CrossRef] [PubMed]
170. Adams, M.A.; Dolan, P.; Hutton, W.C. The stages of disc degeneration as revealed by discograms. *J. Bone Jt. Surg. Br.* **1986**, *68*, 36–41.
171. Pathria, M.; Sartoris, D.J.; Resnick, D. Osteoarthritis of the facet joints: Accuracy of oblique radiographic assessment. *Radiology* **1987**, *164*, 227–230. [CrossRef] [PubMed]
172. Modic, M.T.; Masaryk, T.J.; Ross, J.S.; Carter, J.R. Imaging of degenerative disk disease. *Radiology* **1988**, *168*, 177–186. [CrossRef] [PubMed]
173. Modic, M.T.; Steinberg, P.M.; Ross, J.S.; Masaryk, T.J.; Carter, J.R. Degenerative disk disease: Assessment of changes in vertebral body marrow with MR imaging. *Radiology* **1988**, *166*, 193–199. [CrossRef] [PubMed]
174. Mok, F.P.; Samartzis, D.; Karppinen, J.; Fong, D.Y.; Luk, K.D.; Cheung, K.M. Modic changes of the lumbar spine: Prevalence, risk factors, and association with disc degeneration and low back pain in a large-scale population-based cohort. *Spine J.* **2016**, *16*, 32–41. [CrossRef] [PubMed]
175. Thompson, J.P.; Pearce, R.H.; Schechter, M.T.; Adams, M.E.; Tsang, I.K.; Bishop, P.B. Preliminary evaluation of a scheme for grading the gross morphology of the human intervertebral disc. *Spine* **1990**, *15*, 411–415. [CrossRef] [PubMed]
176. Weiner, D.K.; Distell, B.; Studenski, S.; Martinez, S.; Lomasney, L.; Bongiorni, D. Does radiographic osteoarthritis correlate with flexibility of the lumbar spine? *J. Am. Geriatr. Soc.* **1994**, *42*, 257–263. [CrossRef] [PubMed]
177. Pfirrmann, C.W.; Metzdorf, A.; Zanetti, M.; Hodler, J.; Boos, N. Magnetic resonance classification of lumbar intervertebral disc degeneration. *Spine* **2001**, *26*, 1873–1878. [CrossRef] [PubMed]
178. Carragee, E.J.; Han, M.Y.; Suen, P.W.; Kim, D. Clinical outcomes after lumbar discectomy for sciatica: The effects of fragment type and anular competence. *J. Bone Jt. Surg. Am.* **2003**, *85-A*, 102–108. [CrossRef]
179. Thalgott, J.S.; Albert, T.J.; Vaccaro, A.R.; Aprill, C.N.; Giuffre, J.M.; Drake, J.S.; Henke, J.P. A new classification system for degenerative disc disease of the lumbar spine based on magnetic resonance imaging, provocative discography, plain radiographs and anatomic considerations. *Spine J.* **2004**, *4*, 167S–172S. [CrossRef] [PubMed]

180. Wang, Y.; Videman, T.; Battie, M.C. Lumbar vertebral endplate lesions: Prevalence, classification, and association with age. *Spine* **2012**, *37*, 1432–1439. [CrossRef] [PubMed]
181. Rutges, J.P.; Duit, R.A.; Kummer, J.A.; Bekkers, J.E.; Oner, F.C.; Castelein, R.M.; Dhert, W.J.; Creemers, L.B. A validated new histological classification for intervertebral disc degeneration. *Osteoarthr. Cartil.* **2013**, *21*, 2039–2047. [CrossRef] [PubMed]
182. Cunha, C.; Almeida, C.R.; Almeida, M.I.; Silva, A.M.; Molinos, M.; Lamas, S.; Pereira, C.L.; Teixeira, G.Q.; Monteiro, A.T.; Santos, S.G.; et al. Systemic delivery of bone marrow mesenchymal stem cells for in situ intervertebral disc regeneration. *Stem Cells Transl. Med.* **2017**, *6*, 1029–1039. [CrossRef] [PubMed]
183. Jiang, C.; Li, D.P.; Zhang, Z.J.; Shu, H.M.; Hu, L.; Li, Z.N.; Huang, Y.H. Effect of basic fibroblast growth factor and transforming growth factor-β1 combined with bone marrow mesenchymal stem cells on the repair of degenerated intervertebral discs in rat models. *Zhongguo Yi Xue Ke Xue Yuan Xue Bao* **2015**, *37*, 456–465. [PubMed]
184. Li, X.; Zhang, Y.; Song, B.; En, H.; Gao, S.; Zhang, S.; Cai, Y.; Li, Z.J.; Li, C.; Wang, W.; et al. Experimental application of bone marrow mesenchymal stem cells for the repair of intervertebral disc annulus fibrosus. *Med. Sci. Monit.* **2016**, *22*, 4426–4430. [CrossRef] [PubMed]
185. Noriega, D.C.; Ardura, F.; Hernandez-Ramajo, R.; Martin-Ferrero, M.A.; Sanchez-Lite, I.; Toribio, B.; Alberca, M.; Garcia, V.; Moraleda, J.M.; Sanchez, A.; et al. Intervertebral disc repair by allogeneic mesenchymal bone marrow cells: A randomized controlled trial. *Transplantation* **2016**. [CrossRef] [PubMed]
186. Pereira, C.L.; Teixeira, G.Q.; Ribeiro-Machado, C.; Caldeira, J.; Costa, M.; Figueiredo, F.; Fernandes, R.; Aguiar, P.; Grad, S.; Barbosa, M.A.; et al. Mesenchymal stem/stromal cells seeded on cartilaginous endplates promote intervertebral disc regeneration through extracellular matrix remodeling. *Sci. Rep.* **2016**, *6*, 33836. [CrossRef] [PubMed]
187. Thorpe, A.A.; Dougill, G.; Vickers, L.; Reeves, N.D.; Sammon, C.; Cooper, G.; Le Maitre, C.L. Thermally triggered hydrogel injection into bovine intervertebral disc tissue explants induces differentiation of mesenchymal stem cells and restores mechanical function. *Acta Biomater.* **2017**. [CrossRef] [PubMed]
188. Acosta, F.L., Jr.; Lotz, J.; Ames, C.P. The potential role of mesenchymal stem cell therapy for intervertebral disc degeneration: A critical overview. *Neurosurg. Focus* **2005**, *19*, E4. [CrossRef] [PubMed]
189. Clarke, L.E.; Richardson, S.M.; Hoyland, J.A. Harnessing the potential of mesenchymal stem cells for IVD regeneration. *Curr. Stem Cell Res. Ther.* **2015**, *10*, 296–306. [CrossRef] [PubMed]
190. Gou, S.; Oxentenko, S.C.; Eldrige, J.S.; Xiao, L.; Pingree, M.J.; Wang, Z.; Perez-Terzic, C.; Qu, W. Stem cell therapy for intervertebral disk regeneration. *Am. J. Phys. Med. Rehabil.* **2014**, *93*, S122–S131. [CrossRef] [PubMed]
191. Hiyama, A.; Mochida, J.; Sakai, D. Stem cell applications in intervertebral disc repair. *Cell. Mol. Biol.* **2008**, *54*, 24–32. [PubMed]
192. Bostelmann, R.; Bostelmann, T.; Nasaca, A.; Steiger, H.J.; Zaucke, F.; Schleich, C. Biochemical validity of imaging techniques (X-ray, MRI, and dGEMRIC) in degenerative disc disease of the human cervical spine-an in vivo study. *Spine J.* **2017**, *17*, 196–202. [CrossRef] [PubMed]
193. Fazzalari, N.L.; Costi, J.J.; Hearn, T.C.; Fraser, R.D.; Vernon-Roberts, B.; Hutchinson, J.; Manthey, B.A.; Parkinson, I.H.; Sinclair, C. Mechanical and pathologic consequences of induced concentric anular tears in an ovine model. *Spine* **2001**, *26*, 2575–2581. [CrossRef] [PubMed]
194. Melrose, J.; Shu, C.C.; Dart, A.; Martin, J.; Bell, R.; Little, C.B. Prevention and treatment of intervertebral disc degeneration with bone marrpw derived stem (stromal) cells-an in vivo study in sheep. *Glob. Spine J.* **2014**, *4*, s-0034.
195. Shu, C.; Dart, A.; Clarke, J.; Martin, J.; Little, C.B.; Melrose, J. Prevention and treatment of intervertebral disc degeneration with bone marrow derived stem (stromal) cells-an in vivo study in sheep. *Osteoarthr. Cartil.* **2014**, *22*, S28–S29. [CrossRef]
196. Castaneda, S.; Roman-Blas, J.A.; Largo, R.; Herrero-Beaumont, G. Osteoarthritis: A progressive disease with changing phenotypes. *Rheumatology* **2014**, *53*, 1–3. [CrossRef] [PubMed]
197. Driban, J.B.; Sitler, M.R.; Barbe, M.F.; Balasubramanian, E. Is osteoarthritis a heterogeneous disease that can be stratified into subsets? *Clin. Rheumatol.* **2010**, *29*, 123–131. [CrossRef] [PubMed]
198. Knoop, J.; van der Leeden, M.; Thorstensson, C.A.; Roorda, L.D.; Lems, W.F.; Knol, D.L.; Steultjens, M.P.; Dekker, J. Identification of phenotypes with different clinical outcomes in knee osteoarthritis: Data from the Osteoarthritis Initiative. *Arthritis Care Res.* **2011**, *63*, 1535–1542. [CrossRef] [PubMed]

199. Kraus, V.B.; Blanco, F.J.; Englund, M.; Karsdal, M.A.; Lohmander, L.S. Call for standardized definitions of osteoarthritis and risk stratification for clinical trials and clinical use. *Osteoarthr. Cartil.* **2015**, *23*, 1233–1241. [CrossRef] [PubMed]
200. Loughlin, J. Osteoarthritis: All types of trouble–defining OA in the genomic era. *Nat. Rev. Rheumatol.* **2011**, *7*, 200–201. [CrossRef] [PubMed]
201. Riddle, D.L.; Dumenci, L. Modeling longitudinal osteoarthritis data to identify homogeneous subgroups: Opportunities and challenges in a burgeoning literature. *Osteoarthr. Cartil.* **2015**, *23*, 1035–1037. [CrossRef] [PubMed]
202. Talic-Tanovic, A.; Hadziahmetovic, Z.; Madjar-Simic, I.; Papovic, A. Comparison of clinical and radiological parameters at knee osteoarthritis. *Med. Arch.* **2017**, *71*, 48–51. [CrossRef] [PubMed]
203. Waarsing, J.H.; Bierma-Zeinstra, S.M.; Weinans, H. Distinct subtypes of knee osteoarthritis: Data from the Osteoarthritis Initiative. *Rheumatology* **2015**, *54*, 1650–1658. [CrossRef] [PubMed]
204. Shu, C.; Smith, S.M.; Little, C.B.; Melrose, J. Use of FGF-2 and FGF-18 to direct bone marrow stromal stem cells to chondrogenic and osteogenic lineages. *Future Sci. OA* **2016**, *2*, FSO142. [CrossRef] [PubMed]
205. Melrose, J.; Smith, S.M.; Smith, M.M.; Little, C.B. The use of Histochoice for histological examination of articular and growth plate cartilages, intervertebral disc and meniscus. *Biotech. Histochem.* **2008**, *83*, 47–53. [CrossRef] [PubMed]